INVESTIGATION OF NEUROVASCULAR COUPLING WITH MULTIMODAL IMAGING SYSTEM: A FNIRS – EEG STUDY

A Dissertation

Presented to

the Faculty of the Department of Biomedical Engineering

University of Houston

In Partial Fulfillment

of the Requirements for the Degree

Doctor of Philosophy

in Biomedical Engineering

by

Hasan Onur Keles

August 2015

INVESTIGATION OF NEUROVASCULAR COUPLING WITH MULTIMODALITY IMAGING SYSTEM: A FNIRS – EEG STUDY

Hasan Onur Keles

Approved:

Chair Of The Committee
Dr. Ahmet Omurtag, Associate Professor,
Biomedical Engineering Department

Committee Members:

Dr. Yasemin M Akay, Assistant Professor,
Biomedical Engineering Department

Dr. Nuri Ince, Assistant Professor,
Biomedical Engineering Department

Dr. Ting Chen, Assistant Professor,
Biomedical Engineering Department

Dr. Sridhar Madala,
Indus Instrument, Founder and President

Dr. Suresh K. Khator,
Associate Dean,
Cullen College of Engineering

Dr. Metin Akay, Founding Chair,
John S. Dunn Cullen Endowed Professor,
Department of Biomedical Engineering

ACKNOWLEDGMENTS

First and foremost, I would like to thank my advisor, Dr. Ahmet Omurtag for his endless support, knowledge, help and kindness. I always felt that I am lucky to work with Dr. Omurtag. I hope I continue to have opportunities to interact and work with Dr. Omurtag for the rest of my life. I would like to thank Dr. Metin Akay, Dr. Yasemin Akay, Dr. Nuri Ince, Dr. Ting Chen, Dr. Andrei Dragomir and Dr. Sridhar Madala for serving as my committee members. I would especially like to thank my labmates; Haleh Aghajani, Alessio Buccino, Nesrine Aroua and Duong Nguyen. It was great to work with you, my friends. My previous advisors from Boston, I would like to thank Dr. Song Seok Song, Dr. Feng Xu and Dr. Utkan Demirci. I learnt how to do research from you and I always appreciated all your effort you made for me. I would like to thank all the wonderful people who have helped me enormously during my stay in Boston and in Houston.

I would like to acknowledge Raziye Kaya who always supported me during my time here (Thanks Raz!). Dr. Naze Gul Avci, I especially thank her for her support and help during my PhD (we got a PhD together!). I would like to thank Dr. Seda Nur Topkaya for endless support and encouragement.

A special thanks to my family, my father Hamza Keles, my mother Done Keles, my brother Ugur Keles, my sister-in-law Dilek Sezer Keles, my niece Ela Keles and my nephew Efe Keles for all their love, encouragement and endless support. I dedicate my dissertation work to you. It was a long journey and we did it!

INVESTIGATION OF NEUROVASCULAR COUPLING WITH MULTIMODAL IMAGING SYSTEM: A FNIRS – EEG STUDY

An Abstract

of a

Dissertation

Presented to

The Faculty of the Department of Biomedical Engineering

University of Houston

In Partial Fulfillment

Of the Requirements for the Degree of

Doctor of Philosophy

in Biomedical Engineering

By

Hasan Onur Keles

August 2015

ABSTRACT

Technological advances in functional neuroimaging contributed to understanding of the neurovascular coupling in humans over the years, however, the temporal and spatial relationship between large-scale neural oscillations and hemodynamic changes is still not completely understood during the different states and different disease states of the human cortex. It is also still unclear that what type of large-scale neural oscillations that mostly drive to the hemodynamic signal. There has been a need for novel tools and methods in neuroimaging to study neurovascular coupling.

This thesis focused on the development of simultaneous Functional Near-Infrared Spectroscopy and Electroencephalography system (simultaneous fNIRS+EEG) that can be used for the investigation of neurovascular coupling over the whole head. The simultaneous fNIRS+EEG system is then applied to the resting state studies in healthy adult subjects. The results of these resting state experiments are presented. Our finding shows that the EEG signals at various frequencies tend to drive hemoglobin concentration changes with a typical time delay during the resting states. As side studies, the simultaneous fNIRS+EEG is applied to the cognitive task and artifact experiments to evaluate the suitability of the developed system. The results of these task and artifacts experiments are also presented. Our goal was to characterize the basic phenomena through practical, noninvasive methods in order to facilitate the study of diseases known to affect neurovascular coupling, such as traumatic brain injury.

TABLE OF CONTENTS

ACKNOWLEDGMENTS v

ABSTRACT vii

TABLE OF CONTENTS viii

LIST OF FIGURES x

LIST OF TABLES xii

1 CHAPTER 1

1.1 Introduction 1

1.2 Near-Infrared Spectroscopy 4

1.2.1 Introduction 4

1.2.2 Fundamentals of NIRS 5

1.2.3 NIRS Instrumentation 11

1.3 Electroencephalography 12

1.3.1 Introduction 12

1.3.2 Fundamentals of EEG 12

1.3.3 EEG Instrumentation 13

1.3.4 Brain Rhythms 15

1.4 Multimodal Approaches 18

1.4.1 Why multimodal approaches? 18

1.5 Neurovascular Coupling 20

1.5.1 Basics of Neurovascular Coupling and Clinical Significance 20

1.5.2 Neurovascular coupling studies in human 23

2 CHAPTER 25

2.1 Development of Simultaneous fNIRS+EEG 25
2.1.1 Triplet Holder Design and Manufacture 25
2.1.2 Triplet Holder-Measurement Cap Integration 27
2.1.3 NIRS-micro EEG Integration and Synchronization 29
2.1.4 Preliminary Experiments with the simultaneous fNIRS+EEG 32
3 CHAPTER 34
3.1 Artifact and Validation Studies 34
3.1.1 NIRS Artifacts in EEG 34
3.1.2 Facial Muscle Artifacts 35
3.1.3 Validation with Verbal Fluency Task 43
4 CHAPTER 52
4.1 Resting Sate Studies with simultaneous fNIRS+EEG 52
4.1.1 Introduction 52
4.1.2 Study and Experimental Design 53
4.1.3 Analysis 53
4.1.4 Result 56
4.1.5 Discussion and Conclusion 64
5 CHAPTER 68
5.1 General Discussion and Future Work 68
5.1.1 Portable fNIRS+EEG with TBI 69
5.1.2 Simultaneous fNIRS-EEG in mental workload measurement 71
REFERENCES 73

LIST OF FIGURES

Figure Page

Figure 1.1 Specific extinction spectra of HbR, HbO and water 6

Figure 1.2 Schematic demonstration of photons banana shape 8

Figure 1.3 A typical NIRS activation in response to a stimulus. (Onset 2 s) 10

Figure 1.4 Schematic view of human brain. 13

Figure 1.5 General brain waves obtained by EEG..... 15

Figure 1.6 The hemodynamic response during increased activation of neurons. 22

Figure 1.7 Schematic of Neurovascular Coupling. 22

Figure 2.1 Development of triplet holder and basic measurement unit..... 26

Figure 2.2 Triplet Holders-Cap integration 28

Figure 2.3 Basic measurement unit of fNIRS+EEG and synchronized signals..... 28

Figure 2.4 NIRScout device by NIRx detectors, trigger Input and source 29

Figure 2.5: MicroEEG by Biosignal. 30

Figure 2.6 Schematic diagram showing basic features..... 31

Figure 2.7 Power spectrum of the time series recorded from NIRS 32

Figure 2.8 Power spectrum of the time series recorded from EEG 33

Figure 3.1 Overview of NIRS artifact in EEG(starting at approximately t = 268 s) 35

Figure 3.2 Location of facial muscles and electrode locations..... 36

Figure 3.3 Experimental design of artifact experiment 37

Figure 3.4 EEG spectrogram, EEG signal, and HbO/R concentrations at a different 38

Figure 3.5 Monitoring the effects of artifacts with EEG-EMG-fNIRS. 39

Figure 3.6 Experimental design of jaw clenching artifact experiment 40

Figure 3.7 EEG spectrogram, EEG signal, and HbO/R concentrations at a different 41

Figure 3.8 EEG spectrogram, EEG signal, and HbO/R concentrations over the whole... 42

Figure 3.9 Experimental Design of sematic VFT(Task: VFT-W and VFT-P) 44

Figure 3.10 Topographic view of synchronized EEG spectrogram and time series of 46

Figure 3.11 Topographic view of synchronized EEG spectrogram and time series of ... 47

Figure 3.12 Block averaged synchronized EEG-fNIRS in the VFT –P and VFT-W for . 49

Figure 3.13 Block averaged synchronized EEG-fNIRS in the VFT-P and VFT-W..... 50

Figure 3.14 Block averaged synchronized EEG-fNIRS in the VFT-P and VFT-W from 51

Figure 4.1 The frequency and delay dependence of the autocorrelation of EEG power .. 54

Figure 4.2 Example of whole head EEG spectrogram and HbO / HbR time 57

Figure 4.3 One subject wholehead delayed correlations. 58

Figure 4.4 Whole head time delayed correlation maps between EEG power and Hbo.... 60

Figure 4.5 Subjects averaged delayed correlation between EEG power and HbO (left).. 61

Figure 4.6 Regionally segregated and subject averaged delayed correlation 62

Figure 4.7 Same calculation as in Figure 4.6 but for HbR. Single asterix indicates 62

Figure 4.8 Coupling of EEG Alpha power with hemodynamics 64

LIST OF TABLES

Table Page

Table 1.1 Comparison table between fNIRS, FMRI and EEG 19

Table 2.1 NIRS technical properties 29

Table 2.2: MicroEEG Technical Properties 30

Table 4.1 Subject specific characteristics of the delayed correlation 63

1 CHAPTER

1.1 Introduction

In the brain, neural activity drives local blood flow and oxygenation in a process called neurovascular coupling. Both neural and vascular properties must be simultaneously measured in order to investigate neurovascular coupling. Near-infrared spectroscopy (NIRS), measures the changes in the local concentrations of hemoglobin. Neural activity patterns can be observed by electroencephalography (EEG). Neurovascular coupling is a major topic of interest due to its relationship with pathological conditions that include hypertension, stroke, subarachnoid hemorrhage, and traumatic brain injury. Its investigation calls for an ability to track both the neural and vascular aspects of brain function.

The use of functional NIRS (fNIRS) as an independent modality for investigating the adult brain hemodynamics (1-3) as well as infant development (4) is already well investigated. In most fNIRS studies the use of two distinct wavelengths allows the extraction of the concentration changes of oxy- and deoxy-hemoglobin (HbO and HbR) in the outer layers of the human cortex (5-7). Following neural activation local blood flow and volume typically increase on a time scale of seconds, causing a rise in HbO and a decrease in HbR of smaller magnitude. These concentration changes measured by fNIRS closely agree with the blood oxygen level dependent (BOLD) response from fMRI (8-11).

EEG is thought to result primarily from the synchronization of post-synaptic potentials and therefore represent the input to a neuronal population rather than its output of action

potentials (12). Although the underlying process has a time scale on the order of milliseconds, the parts of scalp EEG that are informative about cortical activity generally remain below the gamma frequency range. This is mainly due to interference from muscle electrical activity (13-16). Scalp EEG rhythms (17) have long been used by clinical neurophysiologists in the differential diagnosis of neurological patients (18, 19). However, it is well known that EEG interpretation contains a substantial intuitive component and the accuracy of EEG interpretation is demonstrably low (20). These may well be due to our incomplete knowledge of its underlying mechanisms. An important limitation of EEG lies in the difficulty of resolving and spatially localizing its sources (21). In order to help overcome such limitations and clarify the relationship of EEG to normal and pathological brain function, researchers are increasingly using multi-modal measurements which combine EEG with other methods.

EEG combined with functional magnetic resonance imaging (fMRI) is able to correlate neural activity with a sequence of highly space-resolved images ultimately based on hemodynamics (22-28). Technical progress has also made it possible to combine EEG with fNIRS, another non-invasive method. This method, we refer to as simultaneous fNIRS+EEG, yields similar measurements with lower space but higher time resolution, in a far more practical and cost-effective arrangement (29-35).

Resting state (RS) EEG contains spontaneously occurring patterns with characteristic frequencies and regions on the scalp. These patterns are presumably associated with transient neuronal assemblies that perform various functions linked to information processing (36, 37). Among the most studied frequency bands is the alpha rhythm in the range 8-14 Hz. Easily identifiable in the occipital and parietal areas of awake, eyes-

closed subjects, it was the first EEG pattern to be observed (38). In addition combinations of delta, theta, alpha, beta, and gamma bands have been reported sometimes coexisting and competing in the same area (17, 39, 40) and correlated with RS networks (27, 41, 42). In fact the distribution of the citations of research on EEG frequency bands replicates the power spectrum of the EEG (43).

In this thesis, we have three main aims. The first aim is to develop the non-invasive simultaneous fNIRS+EEG system which can simultaneously track brain's neural and hemodynamic activity over the whole head. Currently, we developed the system which allows us to examine the relationship between the large-scale neural oscillations and the brain hemodynamics in the human cortex. Technical solutions, tools and analysis methods have been developed during the process of combining two different modalities. The second aim is to evaluate the feasibility and the suitability of simultaneous fNIRS+EEG system. With this purpose, the simultaneous fNIRS+EEG system has been tested using cognitive and artifacts tasks. The final aim is to apply simultaneous fNIRS+EEG to investigate neurovascular coupling over the whole head during the resting states. This study will lay the groundwork for an array of planned future projects that seek to establish efficient and inexpensive measures for the purpose of monitoring and diagnosis of abnormalities such as hypertension, stroke, subarachnoid hemorrhage, and traumatic brain injury.

In this thesis, we have five chapters covering three specific aims. The first chapter introduces the fundamental of fNIRS, EEG, Multimodal imaging and Neurovascular coupling. The second focused on the developmental stages of simultaneous fNIRS+EEG system that has been built in our laboratory. In the chapter three, simultaneous

fNIRS+EEG system has been tested with the cognitive task and the results are presented. In the end of chapter three, the artifact characterization experiments have been described. The chapter four describes the application of simultaneous fNIRS+EEG system during the resting states and the results are presented. The final chapter describes the brief general conclusion and future work including the development of portable, wireless fNIRS+EEG system and clinical application of fNIRS+EEG system.

1.2 Near-Infrared Spectroscopy

1.2.1 Introduction

NIRS is an optical measurement modality to non-invasively investigate the blood oxygenation and hemodynamics in humans and animals. This modality is particularly useful in functional neuroimaging measurements because of the relationship between neural and hemodynamic activity in the brain. fNIRS yields local measures of HbO and HbR concentration and is therefore an indicator of metabolic/hemodynamic changes associated with neural activity. NIRS can be performed by placing optodes (sources and detector) over the head. Light sources shine near-infrared light into tissue, and light detectors collect reflected light. The detected light can be used to calculate the blood oxygenation changes associated with the neural activity (5).

In 1977, F.F. Jobsis published the first NIRS study for optical detection in humans. His study reported that NIRS is a feasible non-invasive method for monitoring the concentration of hemodynamic changes in the brain (44). BOLD-based functional fMRI were introduced by several groups in 1992. One year later, Hemoglobin concentration

changes during brain activation were first measured with NIRS in 1993. The four research groups published results and showed the brain activation measurement in response to stimulation with NIRS in the same year (45-48).

1.2.2 Fundamentals of NIRS

NIRS uses light in the near-infrared (NIR) spectral range (~650–950 nm, 'optical window') which can penetrate several centimeters into biological tissue (49). When light is illuminated into tissue, the photons do not simply reflect or transmit through tissue. NIR photons mainly can be absorbed or scattered by the tissue structures and molecules, such as lipids, water or chromophores. The scattering probability of photons is much greater than the absorption probability of photons inside tissue. Since the human head is highly scattering, the near infrared photons change directions and scatter many times. Experimental and model studies showed that a very small fraction of the photons reaches the head surface (approximately one out of every 10^9 photons) (50). Light attenuation is used to calculate the concentration changes of hemoglobin by using the Beer Lambert Law. Light attenuation depends mainly on the absorption and scattering properties of the tissue structures and molecules, such as lipids, water or chromophores.

Chromophores inside tissue, in particular HbO, HbR and cytochrome aa 3 (Cyt aa3), have specific absorption characteristics in the NIR range, and NIRS measures changes in these chromophores within the brain. As stated above, each chromophore has a different extinction coefficient that defines how strongly a chromophore absorbs light at a particular wavelength. The relationship between a specific extinction coefficient ($\mathcal{E}$) is related to the specific absorption coefficient by this formula; $\alpha=\ln(10)\mathcal{E}$. The main

difference between two coefficients is a scaling factor. **Figure 1.1** represents the specific extinction coefficients at a different wavelength for HbO, HbR and water. Chromophores are the main absorber structures in the tissue. Hemoglobins and C. oxidase are the main type of chromophores, which their concentration changes with time and oxygenation status during the measurement. Cytochrome c oxidase varies with oxygenation status, but it does not significantly affect the measurement because the signal of cytochrome c oxidase is much weaker than that of hemoglobin (ten times smaller).

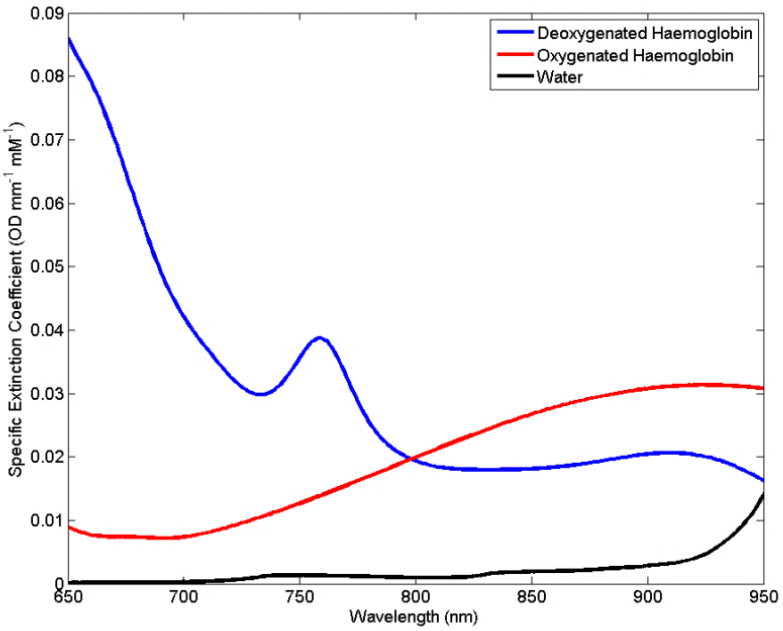

Figure 1.1 Specific extinction spectra of HbR(blue), HbO(red) and water(black) (from UCL Optics Group)

When an oxygen molecule binds to the ferrous iron atom of the heme group of hemoglobin, it is called HbO. If the hemoglobin molecule is bound to nothing, then one is called HbR. NIR photons are strongly absorbed by hemoglobin below 650nm. At the optical window, HbO and HbR have the different absorption spectra which enable us to

calculate changes in HbO and HbR concentration when near-infrared light is applied. 800 nm is an isobestic point, where HbO and HbR have the same absorption coefficient.

Approximately 60% of our total body weight is water which can absorb light significantly in some spectral regions. NIR photons are absorbed weakly by water molecules above 950 nm. Light passes through the skin twice during illumination and reflection. The skin is another light absorber which has three layers: the epidermis, dermis and hypodermis. The epidermis has vesicles containing melanin, which is a very strong absorber in the 300nm-400nm. At the near infrared light, the specific extinction coefficient is constant. It doesn't have a significant effect on the measurement since the attenuation doesn't vary with time. Finally, hair is an important absorber due to the presence of melanin that gives it color. Besides absorption properties of hair, hair is very good scatterer. Dark hair needs to be displaced aside in order to improve signal to noise ratio (51).

1.2.2.1 Banana Shaped Sampling Region

The photons change directions and scatter many times when they travel through tissue, and they follow the curved path which is called "banana shaped" from light source to detector over the head (**Figure 1.2**). Each measurement channel is created by a source a detector placed over the head. The distance between sources and detectors should be at least 2 cm. NIRS signals are assumed to originate from the centered area between the sources detectors (52).

The separation between sources and detectors is important since it defines the depth of penetration in the cortex. If the distance is larger between sources and detectors, the arc

of the banana-shape will be larger which will get information from deeper in the cortex (**Figure 1.2**). While determining the distance source and detectors, the spatial resolution of the measurement and sufficient signal quality must be considered. Generally, a distance of 30-35 mm is considered optimal, and the sensing depth into the adult human head is on the order of 15-25 mm.

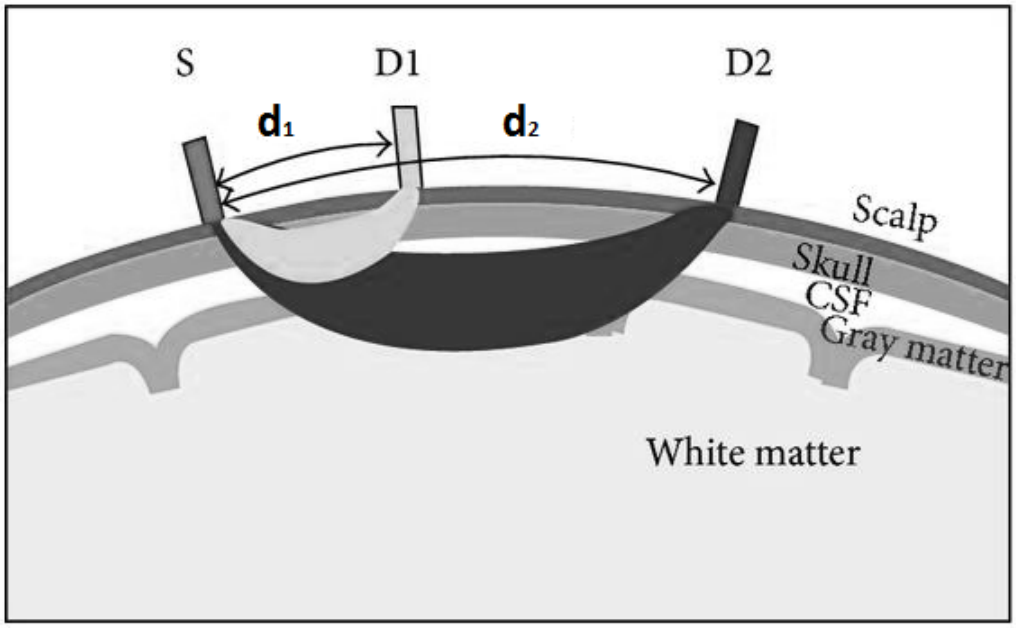

Figure 1.2 Schematic demonstration of photons banana shape(114) S:Source D:Detectors

1.2.2.2 Modified Beer-Lambert Law

The Beer-Lambert Law states that the concentration of chromophores in tissue can be related to the light attenuation. The law considers that that the relationship between light attenuation and concentration of chromophores is a linear. The Beer-Lambert law is defined as (53):

$$A = \log\left(\frac{I}{I_0}\right) = \varepsilon.C.d \ , \qquad \text{(1-a)}$$

Where (A) is the light attenuation, is the logarithmic ratio of two intensity; Io is the intensity of the incident light, I is the intensity of the transmitted light, C(M) is the concentration of a absorber, Ɛ is the molar extinction coefficient($mM^{-1}cm^{-1}$) and d(cm) is the distance that light travels(the inter-optode distance). If there are more than one absorber in the medium, the beer lambert law can be written as

$$A = [\varepsilon_1.C_1 + \varepsilon_2.C_2 + ... + \varepsilon_n.C_n].d \ . \qquad \text{(1-b)}$$

The aim is to find C1,.., Cn in the above equation. A is the experimentally measured (at x wavelengths for x chromophores of interest), d is the distance between source and detector. Ɛ from the literature has been shown previously for HbO and HbR.

Scatter is considered to be zero in the Beer-Lambert Law. Human tissue is inhomogeneous and a highly scattering medium, such that the Beer-Lambert law cannot be used for biological tissue. When a highly scattering medium is considered, the differential path length factor and the scattering losses (G) must be considered. The modified Beer-Lambert Law (54) can be written as

$$A = \log\left(\frac{I}{I_0}\right) = \varepsilon.C.d.DPF + G \, . \qquad \text{(1-c)}$$

If we consider time (t) and wavelength (λ) can be shown as

$$A(t,\lambda) = \log\left(\frac{I(t,\lambda)}{I_0(t,\lambda)}\right) = \sum_i \varepsilon(\lambda).C_i(t).d.DPF(\lambda) + G(\lambda) \, . \qquad \text{(1-d)}$$

DPF defines the increase in optical path length due to scattering in the tissue. The light travels in a longer path due to the scattering. During the calculation, it is assumed that G is not time-dependent; the change in scattering can be neglected when compared with changes in absorption. As result, when considering the change of attenuation ΔA between

the initial time point t_o and a time point t_1 the factor G(λ) is canceled out where $\Delta c_i = c_i(t_1) - c_i(t_0)$. The concentration changes of hemoglobin can be shown as

$$\Delta A(\Delta t, \lambda) = \log\left(\frac{I(t,\lambda)}{I_0(t,\lambda)}\right) = \sum_i \varepsilon(\lambda).\Delta C_i(t).d.DPF(\lambda). \qquad \text{(1-e)}$$

During the recording, DPF cannot be measured directly since the tissue properties cannot be determined absolutely with CW NIRS. As a result, an absolute calculation of chromophore concentration cannot be obtained; only changes in concentration of chromophores can be measured with NIRS with several assumptions.

The hemodynamic response is slow in response to neural stimulation. Hemodynamic response will begin at 2-3 seconds after the onset of neural stimulation. **Figure 1.3** showed the typical hemodynamic response measured by NIRS. Following neural activation local blood flow and volume typically go up on a time scale of seconds, causing a rise in HbO and a decrease in HbR of smaller magnitude (55). Task type, task duration and subject group are closely associated to the hemodynamic response.

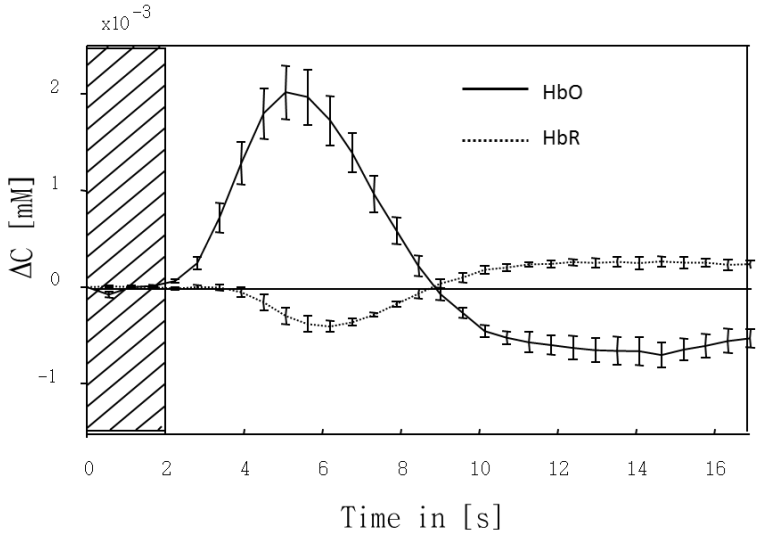

Figure 1.3 A typical NIRS activation in response to a stimulus (Onset 2 s).

1.2.3 NIRS Instrumentation

The last decade has been an exceptionally good one for improving NIRS devices and instrumentations. New companies were involved in development of NIRS instrumentations and NIRS software development (4). Currently, the continuous wave version of NIRS is extensively used in the research and clinical settings due to its price and simplicity (5). Basically, CW-NIRS measures the light intensity of diffusely reflected light. NIRS systems use laser/LED sources to shine light on the tissue at a constant intensity and uses detectors to measure the intensity of diffusely reflected light continuously.

For CW-NIRS, each source should have at least two distinct wavelengths to allow for discrimination of the HbO and HbR. Two wavelengths (760-850nm) will be emitted simultaneously and distinguished by modulation, each at different frequencies. Source illumination over the head can be in sequence or in parallel. NIRS sources can be laser diodes or light emitting diodes (LED). Fiber optics is used to guide the transmitted reflected light from the recording site over the whole head. Photodiodes converts a light signal into an electrical signal. The sources and detectors should be located with several cm distance over the tissue in order to make sure near infrared light will go deep enough to reach the cortex, and the reflected light will be collected sufficiently. Continuous wave NIRS can be used for optical tomography (3D image) by using a sufficient number of probes (high density) with different source-detector separation and arrangements (56, 57). The production of three dimensional images will have information about the depth of chromophore concentration changes.

1.3 Electroencephalography

1.3.1 Introduction

Electroencephalography (EEG) results directly from the electrical activity of cortical and subcortical neurons with a sub-millisecond temporal resolution. The first EEG recording in humans was conducted by Hans Berger in 1924 (38). His study was the first to show the presence of rhythmic activity oscillations (10Hz-Alpha) during a relaxed state without any mental activity. The importance of his study is to show that the EEG oscillations may be associated with mental activity. EEG is the oldest non-invasive method for the diagnosis of neurological diseases. Meanwhile, EEG is the gold-standard method in the diagnosis of epilepsy and seizures (58). Large-scale neural oscillatory activity, which can be recorded with EEG, is classified by characteristic frequency bands such as theta (4–7 Hz), alpha (8–12 Hz), beta (15–12 Hz) and gamma (30 Hz) oscillations (19). These brain rhythms contain relevant information on the ongoing neuronal processing in a specific brain area (21, 58).

1.3.2 Fundamentals of EEG

EEG oscillations recorded via scalp electrodes are thought to be produced by both excitatory and inhibitory PSP's in the cortical pyramidal neurons(19). The single neuron depolarization doesn't produce a detectable signal over the head. During the generation of an EEG oscillation, it is assumed that tens of thousands of synchronized pyramidal cortical neurons are involved. Their dendritic trunks are coherently orientated, or parallel with each other (and perpendicular to the cortical surface) so as to allow sufficient

summation and propagation to the scalp (58) Importantly, although subcortical contributions to scalp-recorded EEG have been reported in the literature (18,58), cortical macrocolumns (or modules) are still thought to be the major contributing force behind EEG signals (19).

As discussed, the mechanisms which underlie the EEG reading are not fully understood as yet, but the interactions between the thalamic and cortical networks are believed to play a key role in rhythmical EEG processes. Indeed, this rhythm, much like that of any waveform is described and characterized by its frequency, amplitude and locational attributes.

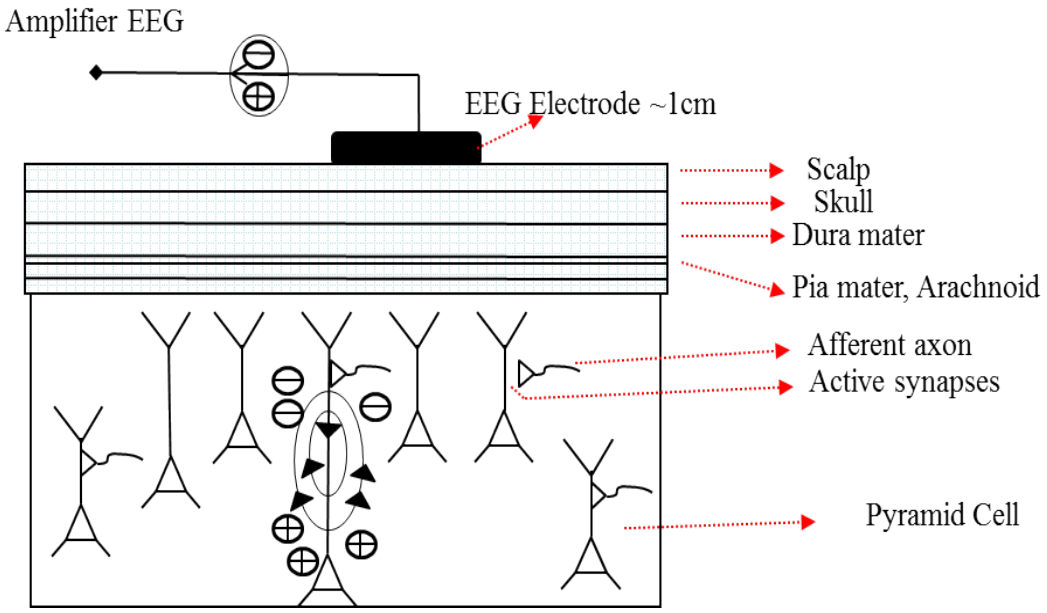

Figure 1.4 Schematic view of human brain.

1.3.3 EEG Instrumentation

EEG is a non-invasive measurement imaging modality. Scalp EEG is performed with the use of sensory electrodes (including a reference electrode and a ground electrode)

which are placed over a person's scalp. Voltages differences between the electrodes and the reference point is measured and amplified. Typically, electrodes are just small metal cups which are highly conductive and made of non-reactive metals like gold or coated silver (Ag/AgCl). Measuring electrical potential requires a current to flow between two points and any interference of flow can produce serious affects to the reading which decreases accuracy in the results. Therefore, it is important to obtain low impedance between the sensing and reference electrodes; this is achieved by making fixation to the scalp as strong as possible. This often means removal of dead skin cells by abrasion, and the addition of a conductive gel to the base or inside of the electrodes. A desired rate of impedance between electrodes is less than 5 k to allow a good signal-to-noise ratio (19). The quality of the electrode contact to the scalp is often measured by its electrical impedance but there are also situations where signal-to-noise ratios have exceeded 5 k by impedance standards yet still have produced acceptable results. That is dependent on the input interference produced by the EEG amplifier itself. Equally, one may establish excellent scalp contact during the EEG but the electrical characteristics of the recording room may still provide noisy interference.

Nineteen sensory electrodes are used in a clinical EEG, which are placed intermittently across the scalp surface in a standard formation defined by the 10-20 international system of placement. The system provides for 19 main electrode sites by 10% and 20% divisions of nasion-to-inion sagittal and left-to-right pre-aurical coronal distances (59).

1.3.4 Brain Rhythms

The signals measured with EEG are called “brainwaves”. They are usually classified into frequency bands. Common bands divide the frequency range between 8-13 Hz for alpha (α) waves, 14-80 Hz for beta (β) waves, 4-7 Hz for theta (θ) waves, and under 3.5 Hz for delta (δ) waves (Figure 1.5). For adult subjects one would expect to see normative EEG oscillations between range from 0 to 100 microVolts in intensity and from 0+ to 80 Hz in frequency(58).

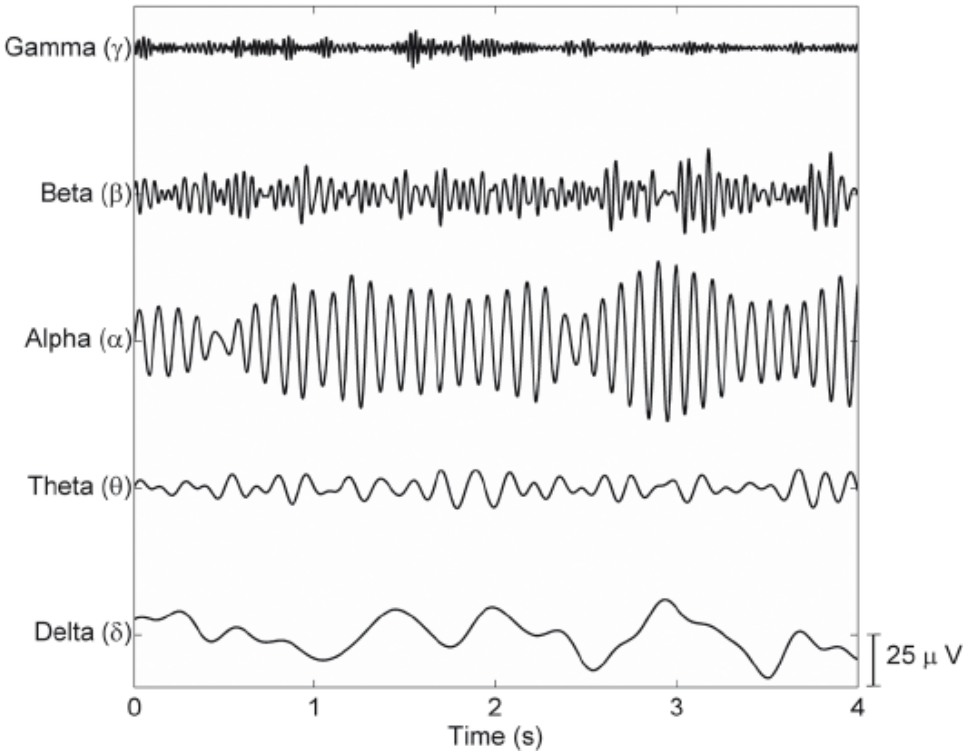

Figure 1.5 General brain waves obtained by EEG

Temporal resolution shown in milliseconds by the EEG, allows us to discover not only increases and decreases in EEG activity as a result of demanding tasks but also to distinguish between inhibitory functions and excitatory activity. Generally, low frequencies such as delta and theta show as large synchronized amplitudes but EEG

frequencies, being beta and gamma etc. shows smaller amplitude denoting a high amount of desynchronization in the sub-layer neuronal activity. From here, a review of different EEG oscilations and their roles are discussed.

1.3.4.1 Delta Rhythm

Low-frequency activity in normal humans is presented by the Delta oscillations (1-4 Hz). They are observed during deep sleep and during infancy. The power of delta waves has been shown to increase tumors and brain lesion (19). This is also the case during anesthesia (60) and periods of sleep (61, 62). The main activity within infants' brains during their first two years of life is delta. Its activity, along with theta activity, decreases as subjects' age, and the faster alpha and beta waves increase activity in a linear fashion throughout lifespan (19). Together, this suggests that delta rhythms are mostly inhibitory in nature.

1.3.4.2 Theta Rhythm

The slow activity is known as theta, which is between 4-8 Hz. This is also usually seen during sleep in wakefulness. There have been two theta types observed in adults. First type indicates widespread distribution across the scalp, associated to drowsiness or impaired processing. Second type is known as a frontal midline theta activity (63). This is essentially comprised of focused attention, extra mental effort and processing. Studies have further linked this to the anterior cingulate cortex as a kind of generator for this frontal midline theta (19, 63, 64). Another study gave consistent support for this during an integration of both electrical (EEG) and metabolic (PET) measurements. Pizzagalli

and his colleagues (65) showed that the anterior cingulate cortex had significant positive correlations to both theta current density and glucose metabolism; along with being the the largest region of such effect.

1.3.4.3 Alpha Rhythm

Alpha oscillations are observed to dominate the EEG during quiet and relaxed wakefulness. Indeed, these alpha oscillations can be obtained for all three of these systems: visual, auditory and sensory-motor. Findings showed that desychronization in the alpha bands is closely related to cognitive and motor processing of the human brain (66, 67). It's been theorized that thalamo-cortical feedback loops and strengthened thalamic interconnections are prerequisites for cortically produced alpha rhythms (68). But the functional relevance of alpha rhythms is still under investigation. Using a number of studies focused on the links between alpha rhythm and many types of cognitive tasks, it is considered to be a 'multifunctional' rhythm. There is also a following for the idling theory that amplitude of the alpha rhythm is actually relatable to the cortical activation; i.e. an increase in alpha-power and its synchronization is linked to cortical and behavioral deactivation or perhaps inhibition (69). Findings showed that alpha rhythm is not only reflecting an "idle" state of human cortex. It also involves the several cognitive processes such as perceptual learning and memory (70, 71).

1.3.4.4 Beta Rhythm

H. Berger observed the beta activity in normal adult in 1924. It is defined as oscillations of 13 Hz-30Hz. Adults have amplitudes of 10-20 microvolt, and it presents as a symmetrical fronto-central display usually during intense mental activities. Along with

this view, a beta rhythm study has seen activity increase with attention and cortical processing (72). Together, the findings generally show that beta increases as a reflection of excitatory activities much like arousal and deeper focus (19, 72).

1.3.4.5 Gamma Rhythm

Under different stimulation of the visual cortex, normal neuronal activity ranges from 35-70 Hz). It has been linked to encoding and binding of stimulus activity and importantly to attention (73), arousal object recognition (74) and learning and memory (75). There is still debate as to where gamma activity originates from, however it seems to be quite crucial (31, 76). Whether these oscillations come from intrinsic membrane properties or from neocortical excitatory/inhibitory style circuits (77).

1.4 Multimodal Approaches

1.4.1 Why multimodal approaches?

The functional activity of the human brain can be observed with various imaging techniques including fMRI, fNIRS and EEG. Each of these modalities has its advantages and disadvantages. Compared to fMRI, fNIRS offers the advantages of a good temporal resolution, small size, and portability, less motion artifacts sensitivity, relatively inexpensive and natural recording conditions. fNIRS provides information about both HbO and HbR concentration changes however, fMRI only measures the BOLD signal which is associated with the concentration of HbR. There are also several disadvantages of fNIRS imaging; the limited penetration depth, low signal-noise ratio, the sensitivity of the superficial tissue effect the signal noise ratio is low (5). For fNIRS, the penetration depth is about 2cm which only allows recording from the cortex. Extra-cerebral effect

can be diminished or enhanced by using the sophisticated instruments or superficial algorithms (78, 79). EEG has a higher temporal resolution (millisecond) compared to fNIRS and fMRI. fNIRS enables us to measure the subject populations with all experimental paradigms that are not suitable for fMRI. The strengths and the weaknesses of fNIRS compared with other functional imaging modalities are shown in **Table 1.1**.

Table 1.1 Comparison table between fNIRS, FMRI and EEG

		fNIRS	fMRI	EEG
Fundamentals of techniques	Signal origin	Optical property Absorbance and Scattering	Magnetic Property	Synchronized Neurons Activity
	Measurement Area	Surface of the cortex	Whole brain	Surface of the cortex
	Measurement Property	HbO-HbR Changes	HbR Changes	Postsynaptic potentials
	Time Resolution	1	2-3	0.01
	Spatial Resolution	20	5	20
Instrument	Size	Small	Large, Fix	Small(microEEG)
	Portability	Yes	No	Yes(microEEG)
	Cost	100,000-400,000 USD	Several million USD	30,000-150,000 USD
Other Settings	Invasiveness	No	No	No
	Body Movement	Tolerable	No	No
	Clinical Application	Medium	Very High	High

Individual imaging techniques provide only limited information about neurovascular coupling due to the complexity of the relationship between neural activity and localized hemodynamic response. In order to make further progress, multimodality approaches are needed, which combine the advantages of individual imaging techniques (e.g., high temporal resolution of EEG) and mitigate their limitations (e.g., volume conduction).

During the last two decades, multimodal imaging became increasingly important in neuroscience due to the complexity of the investigated brain systems.

Despite the many technical and methodological difficulties (e.g., electromagnetic interference), simultaneous fMRI+EEG recording and analysis has been used extensively in many neuroscience laboratories in order to study neurovascular coupling, resting state networks and epilepsy (80). The improvement of epileptic seizure location is the first clinical interest that investigated by fMRI+EEG in 1993 (81). The use of fMRI-EEG is limited with big research facilities due to the large size of EEG-fMRI instrumentation.

fNIRS technology is rapidly growing and developing. However, there is no standardized processing and analysis tools in order to implement in combined experiments. New tools methods and novel approaches are critically needed to facilitate the development of simultaneous fNIRS+EEG. fNIRS has powerful features that make it possible to perform examinations of the functional status of the cortex in clinical offices and under relatively naturalistic environments. fNIRS-EEG are complementary imaging modalities and therefore an important resource and strong candidates for studying aspects of neurovascular coupling and its relationship with pathological brain physiology as well as the mechanisms underlying the BOLD signal.

1.5 Neurovascular Coupling

1.5.1 Basics of Neurovascular Coupling and Clinical Significance

In the brain, neural activity is closely related to cerebral blood flow (CBF). When the neural activity occurs within a localized brain region, blood will flow to the localized brain region in order to meet the increased demand of glucose and oxygen. It is a well-

regulated system that is called Neurovascular Coupling (82) (**Figure 1.6**). It is critical to supply oxygen and nutrients to neurons for their function. The regulation of hemodynamic activity involves the coordinated relationship of neurons, glia cells, and vascular cells while the brain activation (**Figure 1.7**). The neural activity- hemodynamic coupling is directly controlled via various biological signaling pathways. Metabolic factors (CO2, K+, nitric acid, adenosine) and neurotransmitters are involved in controlling the neurovascular coupling. The relationship between neurovascular components forms the theoretical basis for hemodynamic based imaging of brain activity. The neurovascular system and its relationship with the pathology of several neurological diseases are currently under investigation (117). The relationship between neural activity and hemodynamic activity can be altered in brain disorders, and the resulting homeostatic unstability may contribute to brain disease. Impairment of neurovascular system has been shown as a sign factor in several neurological diseases such as Alzheimer's disease, major depressive disorders, ischemic stroke (82, 83).

Many laboratories focused on mild traumatic brain injury (mTBI) and its relations with neurovascular coupling and functional connectivity (84-87). The quantitative whole-head monitoring investigation of neurovascular coupling is important for eliciting measures related to mTBI because of implications of this disease for reduced cerebral perfusion, decreased capillary diameter, and higher reactivity of blood vessel smooth muscles. Investigation of neurovascular coupling might open the new windows for drug development, diagnostic of neurological diseases as well as increase our understanding of the mechanism of the neurovascular system. There is evidence that neurovascular coupling is affected by aging, anesthesia, and diseases including depression, stroke,

hypertension, Alzheimer's, epilepsy, subarachnoid hemorrhage, and traumatic brain injury (88-91).

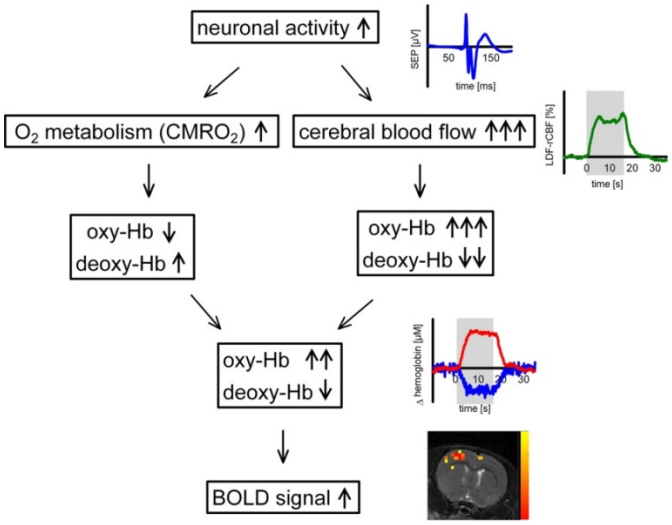

Figure 1.6 The hemodynamic response during increased activation of neurons (112).

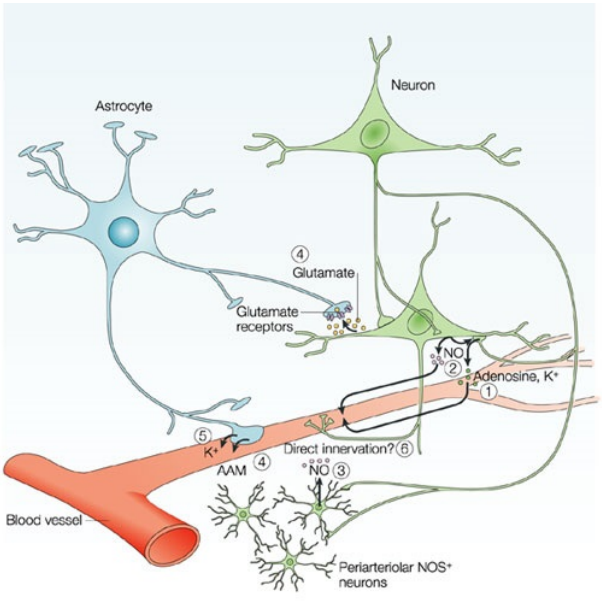

Figure 1.7 Schematic of Neurovascular Coupling (113).

1.5.2 Neurovascular coupling studies in human

The simultaneous recordings of fMRI/fNIRS+EEG provide high spatial and high temporal investigation of neurovascular coupling. In the last decade, numerous papers have been published on multi-modal approaches involving fMRI; there have been far fewer explorations of multimodal studies of fNIRS-EEG. Most studies have been focused on understanding neurovascular coupling during the resting state and the stimulus related states.

Resting state studies mostly focused on the investigation of relationship between the alpha power and hemodynamics. Dr. Mark S. Cohen and his colleagues (28) examined the relationship between alpha power and the hemodynamic response using simultaneous fMRI-EEG during the resting state. F.H. Lopes da Silva's group (92) also examined the relationship between the alpha power and the hemodynamic response. Both studies showed that the strong correlation exist between neural activity and hemodynamic response. Based on the fMRI/EEG studies (92,28), it has been proposed that the amplitude of the alpha rhythm is associated to the level of cortical activation. An increase in alpha power could be related to cortical deactivation or inhibition. An increase in the power of the EEG signal over a specific frequency range generally indicates higher level of synchronized neural firing in those frequencies.

Simultaneous fNIRS+EEG, yields similar measurements with lower space but higher time resolution, in a far more practical and cost-effective arrangement (29-33, 35). M. Moosmann (93) showed that the alpha power correlate with the fNIRS measure of HbR in the occipital cortex by using the simultaneous fNIRS-EEG during the resting state

with the limited number of subjects(n=3) .

Various types of stimulation experimental design were used for the investigation of relationship between electrical activities and hemodynamic. Koch and his colleagues (29) used the flicker-light with fNIRS+EEG and found that vascular response to stimulus is higher when resting alpha frequency is lower. Rosa showed the changes in BOLD are related with changes in the spectral power of neural activity by using fMRI+EEG with the visual flickering checkboard experiment. More complex stimulation studies has been done using combining electrophysiology and fMRI in human, Arne (94) showed correlation between BOLD signal and theta-band activity in the hippocampal areas with spatial navigation experiment. The linear coupling that occurs between fMRI and neuronal amplitude that is observed in the human somatosensory cortex upon stimulation by Arthur and his colleagues (95).

2 CHAPTER

2.1 Development of Simultaneous fNIRS+EEG

2.1.1 Triplet Holder Design and Manufacture

The first task of building the simultaneous fNIRS+EEG is to produce a component for holding the optodes and electrodes. We designed the thin plastic component which holds a triplet of probes (fNIRS source-detector pair approximately 3 cm apart, flanking an EEG electrode) for the purpose of associating the EEG channel closely with a corresponding fNIRS channel. The thin plastic holder has been designed to achieve maximize optical and electrical coupling over the subject's scalp. The distance between optodes and electrodes is restricted by the plastic holder. This holder also increased the mechanical rigidity of optodes-electrodes coupling. The exact dimensions of the plastic holder are shown in **Figure 2.1A.**

fNIRS optodes and EEG electrodes must be in good contact with the scalp in order to ensure appropriate optical contact, signal integrity and low impedance (33). For this reason, the holder must be flexible to suit the hardness and curvature of the scalp. The material of the holder is chosen in a way to satisfy the comfort of the subject. It is necessary to prevent any discomfort that might be experienced by the patient since some experimental paradigms may last for hours. Several prototypes have been produced and tested prior to the final design of holders. These prototypes are shown in **Figure 2.1B** and **Figure 2.1C**. We decided to use the plastic material due to its flexibility and easy customization. With this purpose, Polycarbonate Sheet, Acetate Sheet and Polyoxymethylene have been tested for a triplet holder. Acetate sheet was selected for the

final triplet holder due to its high flexibility, high strength and the light weight. Three different techniques have been used for manufacturing the thin plastic holder prototypes; manual cutting, 3D printing and Laser Cutter. Since the dimensions of the design are relatively small, it is difficult to develop the holder manually. Several holders have been produced with the manual cutting for testing purposes (scissor cutting). The different shapes (square, round, round-flat) of triplet holder have been produced by 3D printer. 3D printing generated a less elastic holder that caused the contact pressure problems. Geometrical stability has been tested with square shape and round shape of the triplet holder. The final design is determined to be square because it provides good geometrical stability (**Figure 2.1D**).

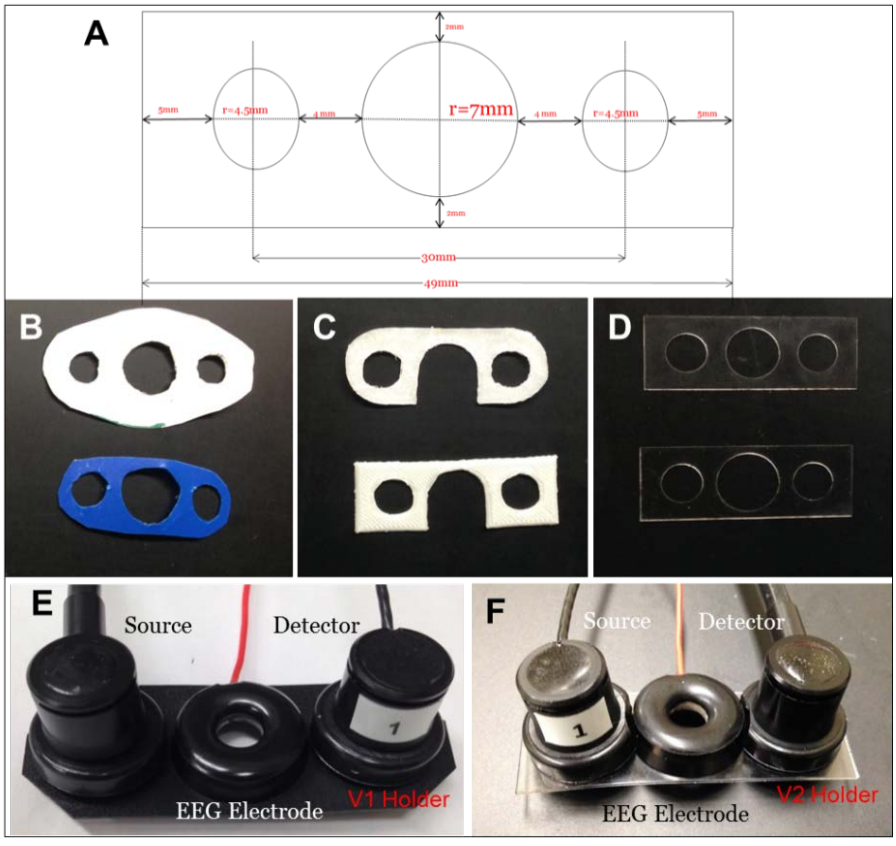

Figure 2.1 Development of triplet holder and basic measurement unit

The final version of the thin plastic component (**Figure 2.1D**) was manufactured by a laser cutter which provided the precise and accurate cutting with unlimited number of holders. The basic measurement unit in multimodal imaging is called “module” that consists of three components: a thin plastic holder, optodes and electrodes (**Figure 2.1E**). The ideal source-detector distance is a critical achieving the greatest possible sensing depth while maintaining a sufficient signal quality (signal-to-noise ratio). Generally, a distance of 30-40 mm is considered optimal. In the first version of a triplet holder (Figure 2.1), 35 mm source-detector separation was used. However, we obtained the fastest calibration and best signal quality with a 30 cm source-detector separation (**Figure 2.1).**

2.1.2 Triplet Holder-Measurement Cap Integration

The second task of my first aim is to modify the cap and to integrate the triplet holder. Currently, there is no widely accepted standard cap for fNIRS-EEG multimodal imaging. There are different caps and holders used by different groups (33). In our study, easy standard cap has been modified using the triplet holders. EasyRcap are made of a stretchable material that suit well with the scalp curvature. The 19 triplet holders were mounted on an extended EEG cap (**Figure 2.2**). We placed electrodes and optodes over the head consistent with the standard international 10-20 system (FP1, FP2, F4, C4, P4, O2, F8, T4, T6, Fz, Cz, Pz, F3, C3, P3, O1, F7, T3, and T5). The standard system ensures that the triplet holders are placed on the location accurately. A ground electrode was placed at Fcz and a reference electrode was placed at Fpz. This standardized system will help to facilitate clinical translation in the future since this standardized location system has been used in clinic for a long time.

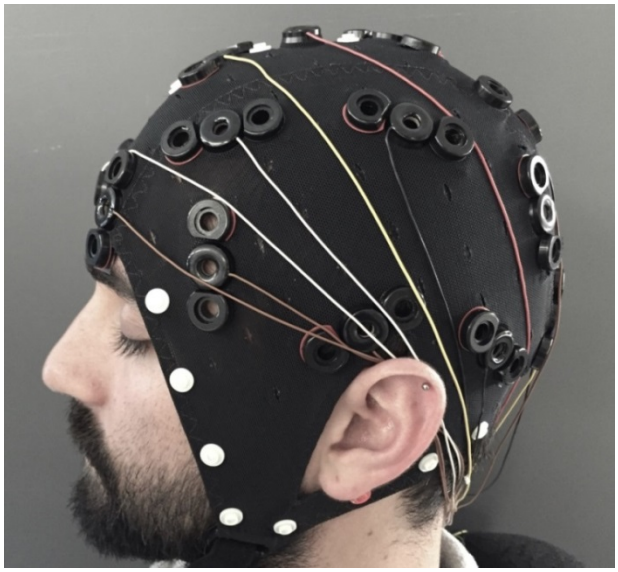

Figure 2.2 Triplet Holders-Cap integration

All extraneous components of Easy^{R} standard cap are extracted. As a result, the light and comfortable cap has been obtained for the multimodal imaging system. The cap is secured by using the extra chin-strap that increased contact pressure over the scalp. Synchronized signals (EEG, HbO, HbR) obtained from sensors in one triplet holder (T6) as shown in **Figure 2.3**.

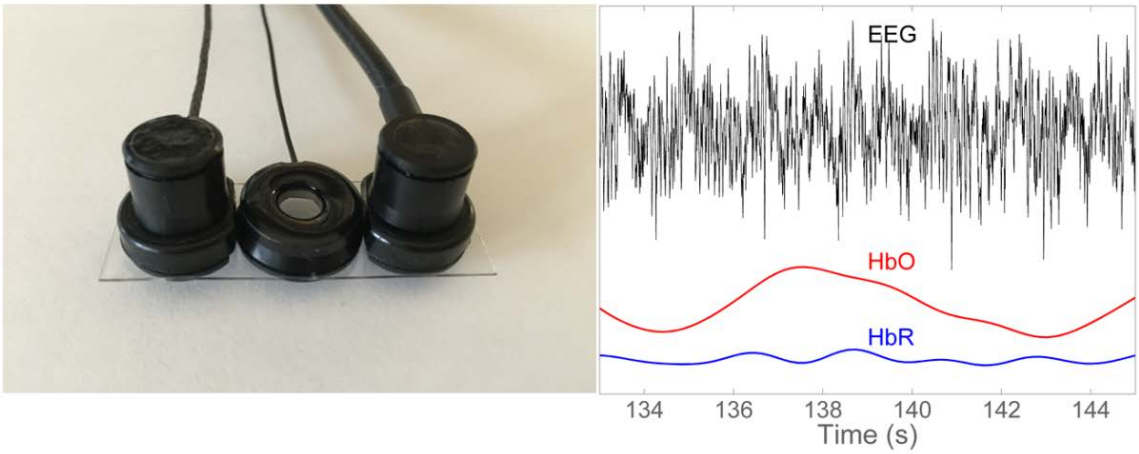

Figure 2.3 Basic measurement unit of fNIRS+EEG and synchronized signals

2.1.3 NIRS-micro EEG Integration and Synchronization

The third step is to integrate and synchronize physically two separate measurement devices. In this study, the NIRScout extended dual-wavelength continuous wave (NIRx Medical Technologies, New York) system was used for NIRS measurements (**Table 2.1**). NIRScout system is one of the most developed NIRS system in the field of neuroimaging. NIRScout is shown in **Figure 2.4**

Figure 2.4 NIRScout device by NIRx Detectors, Trigger Input and Source

Table 2.1 NIRS technical properties

Sensitivity	Better 1pW NEP
Dynamic Range	>90dB
Sensor Type	Si Photodiode
Wavelengths	760nm, 850nm
Power	5mW/Wavelength
Sampling Rate	62.5
Emitter Type	LED

EEG signals were collected using microEEG, a miniature (80 grams), battery operated, wireless data acquisition system (Bio-Signal Group Inc., Brooklyn, New York). microEEG digitizes signals close to the electrode and transmits them via Bluetooth to a nearby standard personal computer running Windows. MicroEEG instrument is show in **Figure 2.5.**

Figure 2.5: MicroEEG by Biosignal. On the left: 32 Channels On the right: 24 Channels

Table 2.2: MicroEEG Technical Properties

A/D Conventer resolution (bits)	16
Voltage resolution	0.15
Maximum imput range	10 mV
Sampling rate	1000 Hz
Bandwith	0.15-500 Hz
Input impedance	>100
Number of channels	32

19 passive EEG ladybird electrodes (Ag/AgCI) and 19 dual-wavelength LED emitters (sources, 760/850nm) and 19 detectors (fiber optic cables) are used for the whole head arrangement. The connector box is designed by Bio-Signal Company in order to connect microEEG amplier and EEG electrodes.

For NIRS-EEG synchronization, the presentation software (Neurobehavioral Systems Inc.) was used to send trigger signals to both the NIRScout and microEEG simultaneously using a LPT splitter cable. The triggers are sent out using a digital TTL signal pulse. These trigger signals are transmitted simultaneously over a cable to the Trigger Input of the NIRScout and microEEG instruments. NIRS and EEG data and event markets are displayed, recorded and stored on the recording PC.

The passive EEG ladybird electrodes are able to plug directly into the box. microEEG has been used in several clinical studies in emergency department and its accuracy is comparable to that of a traditional EEG system that has already been used in hospital. FDA tested and approved microEEG after extensive analysis and clinical studies (96, 97).

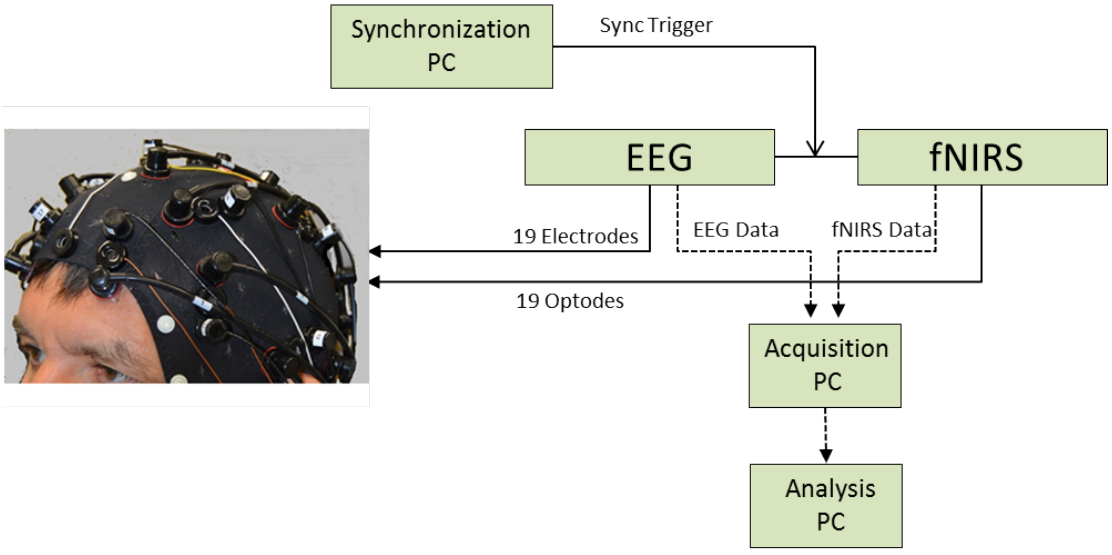

Figure 2.6 Schematic diagram showing basic features of the simultaneous NIRS+EEG

2.1.4 Preliminary Experiments with the simultaneous fNIRS+EEG

The occipital alpha rhythm experiments were performed with 2 human subjects to verify the functionality and signal quality of the developed multimodal imaging system. Recordings were performed while the subject was awake under eyes closed resting conditions. The synchronized signals recorded from 19 modules over the whole head and the synchronized recorded signals are presented in **Figure 2.7**. and **Figure 2.8.**

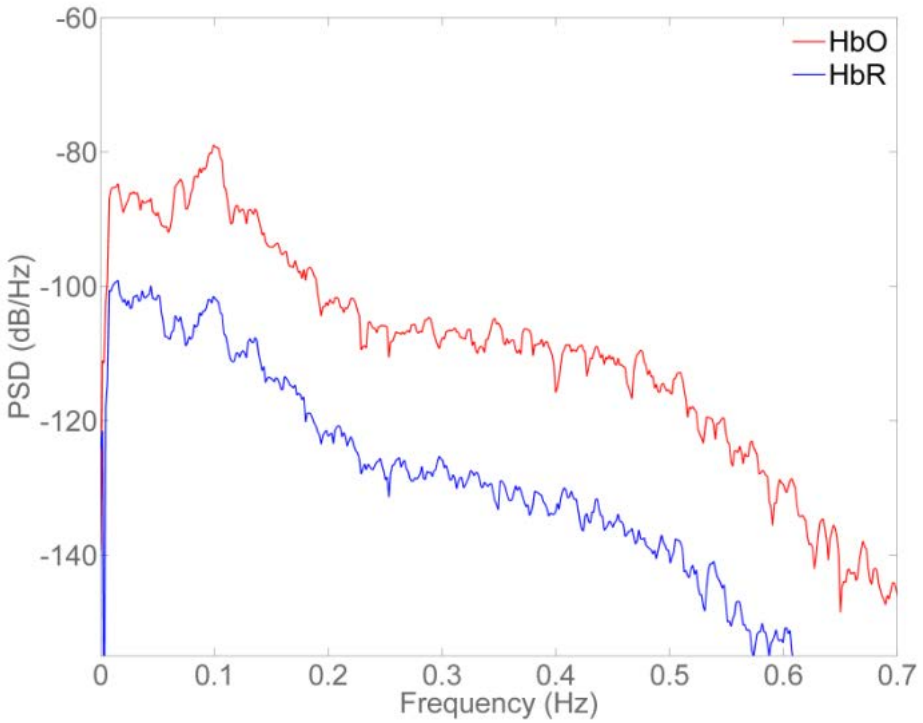

Figure 2.7 Power spectrum of the time series recorded from NIRS

The signals have been preprocessed by bandpass and notch filtering and the Hb concentration changes have been computed by the Modified Beer-Lambert (MBL) law. Before filtering, optical data were manually inspected for movement artifacts. EEG Power Spectral Density (PSD) from all electrodes was computed. The PSDs show the

influence of the notch filter at 60 Hz, the bandpass filter (0.5-80 Hz). As expected, they show varying levels of alpha activity. fNIRS Power Spectral Density from all sensors were also computed. fNIRS signals were preprocessed by bandpass filtering (0.01-0.5 Hz). The fNIRS PSDs typically have a peak at 0.1 Hz (Mayer waves) which is especially pronounced for HbO. The experiment successfully demonstrated that this system has the multimodal recording capability.

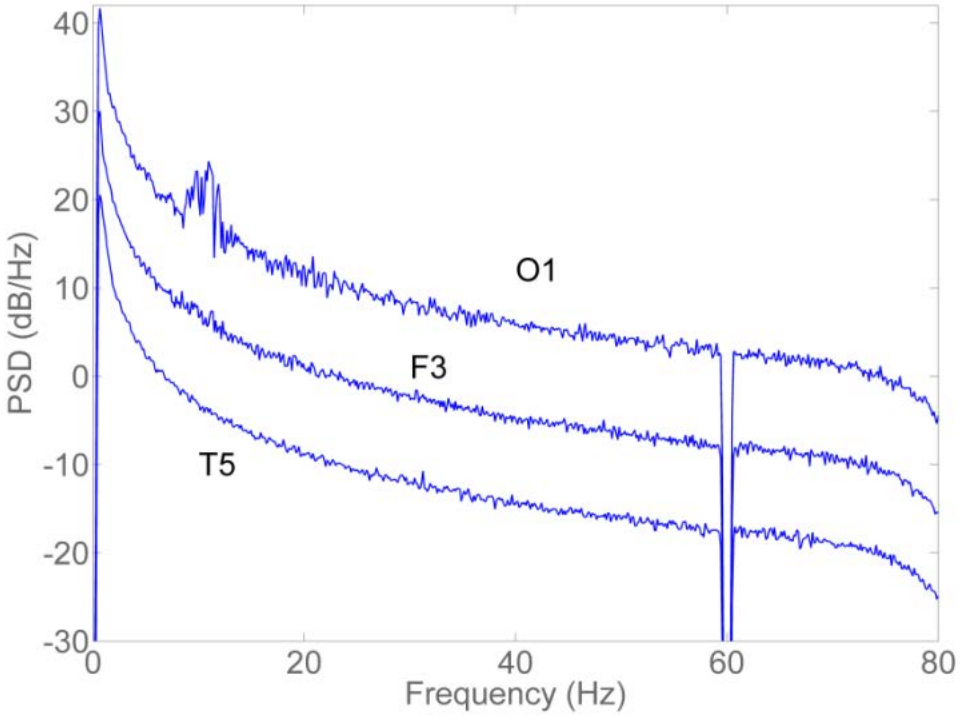

Figure 2.8 Power spectrum of the time series recorded from EEG

3 CHAPTER

3.1 Artifact and Validation Studies

3.1.1 NIRS Artifacts in EEG

Running an experiment with the simultaneous fNIRS+EEG system also revealed issues such as artifacts appearing during simultaneous recording. Simultaneous multimodal recording are often corrupted by different artifacts. In this study, the second aim is to focus on observing and analyzing the artifacts and its characteristic. Our experiments showed that the observed artifacts in the developed simultaneous imaging system can be classified into two categories: NIRS artifacts in EEG and Facial muscle artifacts in NIRS-EEG. During the feasibility studies, the unknown artifacts appeared in EEG time series (**Figure 3.1**). The appeared artifacts have certain frequency (6.25Hz) itself can be recorded by some EEG channels and it is clearly seen in spectral analysis. We noticed that the sampling frequency of the system and noise frequency were matching with each other. We observed that the noise begins when NIRS source cable touched the EEG electrode (starting at approximately t = 268 s). NIRS source causes this 6.25 Hz artifact due to the modulation of the light source power. Our result shows that the artifact can be completely eliminated by careful physical arrangement of the sources and EEG electrodes so that, although they can be nearby, they do not touch. HbO and HbR signals are unaffected. The EEG times series, The EEG power spectrogram hemoglobin concentrations changes (red and blue curves are the HbO and HbR changes, respectively) are shown in **Figure 3.1.** The power spectrogram of the EEG was computed using a 1 s Hamming window with 50% overlap.

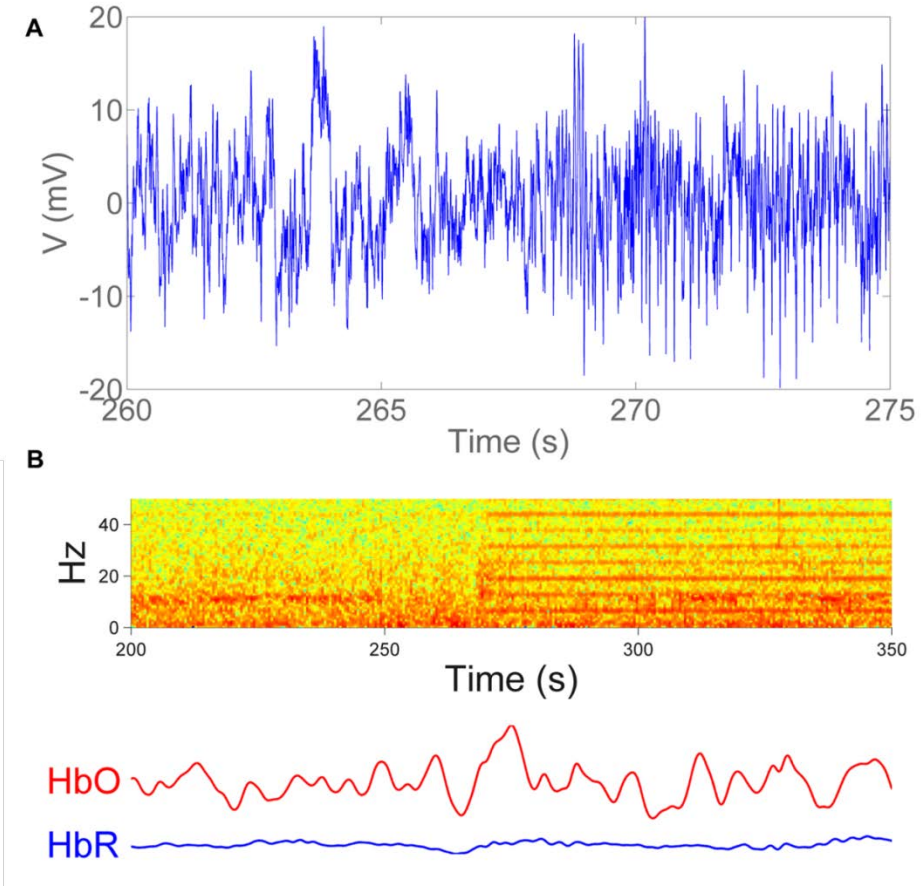

Figure 3.1 Overview of NIRS artifact in EEG (starting at approximately t = 268 s)

3.1.2 Facial Muscle Artifacts

During the feasibility experiments, we observed the high frequency electromyographic activity in EEG and high magnitude hemodynamic activity at the specific channels; F7, F8, T3, T4. Two experiments were designed to investigate the high magnitude activity and electromyographic (EMG) activity on fNIRS and EEG during the simultaneous recording. Our whole head sensor arrangement is positioned to cover the whole head areas including temporal and inferior frontal brain areas. This arrangement also covers the temporalis muscle that is responsible for closing the jaw as it chews (**Figure 3.2**).

Temporalis muscle that covers F7, T3 on the left and F8, T4 on the right side of the head. The temporalis muscle is main sites of myogenic artifacts appearing as burst of fast activity in EEG. Facial EMG contamination of EEG signal is unresolved issues in language studies and BCI research (98). The relation between hemodynamic activity and high frequency activity is under investigation.

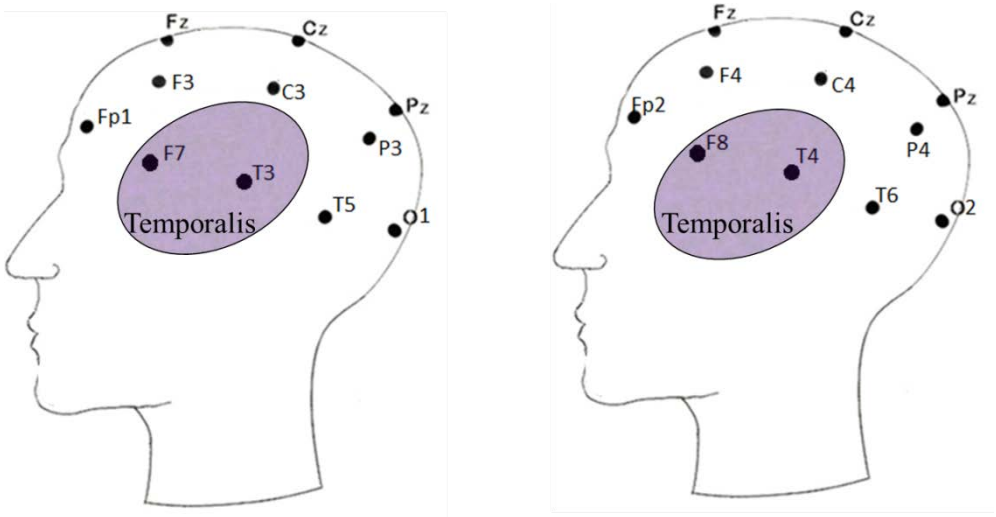

Figure 3.2 Location of facial muscles and electrode locations

In the first experiment, we measured the neural activity and hemodynamic signals over the whole head with the simultaneous fNIRS+EEG while activity of the temporalis muscle was simultaneously assessed with EMG. The experiments included two blocks with each block consisting of jaw clenching, smiling, knitting the brows, each lasting 30 seconds and separated by 30 seconds (**Figure 3.3**). EMG electrodes were placed over the temporalis, masseter and mentalis muscle. We integrated our multimodal imaging system with REFA 128 EMG system (TMS International B.V. The Netherlands) for monitoring EMG. Temporalis muscle is a large muscle located just below the F7 EEG position which

is about 2 cm in ventral direction on the zygomatic bones. Mentalis is a central muscle of the lower lip that raises chin and pushes lower lip upward. EMG electode for mentalis are affixed 0.5cm lateral to the midline. Masseter runs from the temporal bone to the lower jaw.

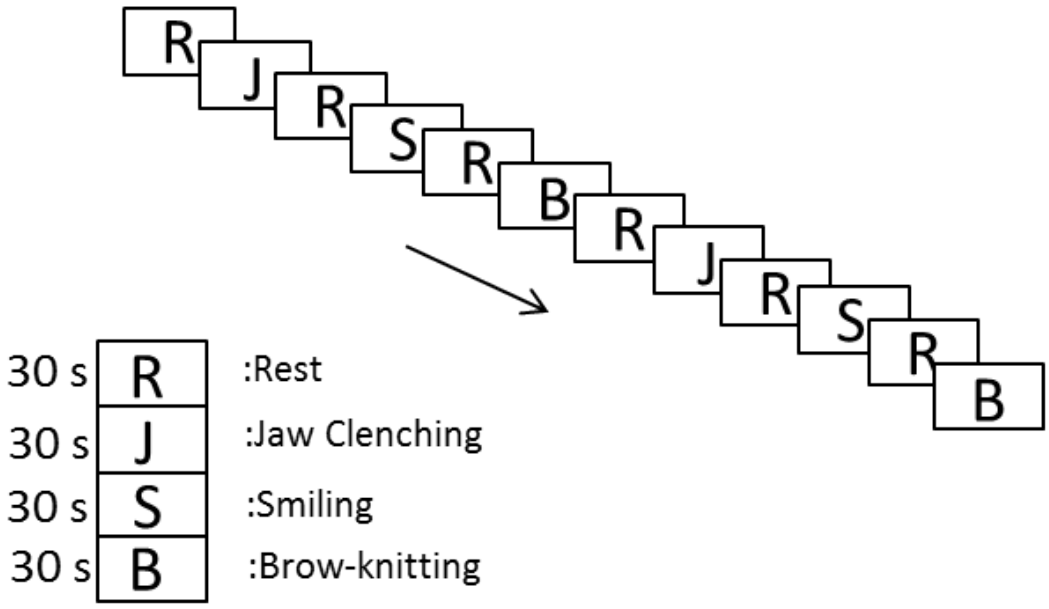

Figure 3.3 Experimental design of artifact experiment

In Figure 3.5, the spectrograms are shown (from top to bottom) of electrodes placed on the subjects Temporalis 1, Temporalis 2, Masseter and Mentalis and recorded with REFA EMG system. During the segment shown the subject was resting with eyes closed and was instructed to clench jaw clenching, smiling and brow-knittings. The results showed that the high frequency components of EEG due to face muscles are picked up by a wide range of EEG electrodes (**Figure 3.4**). By contrast strong hemodynamic activity is confined to sensors over temporalis (T3, F7).

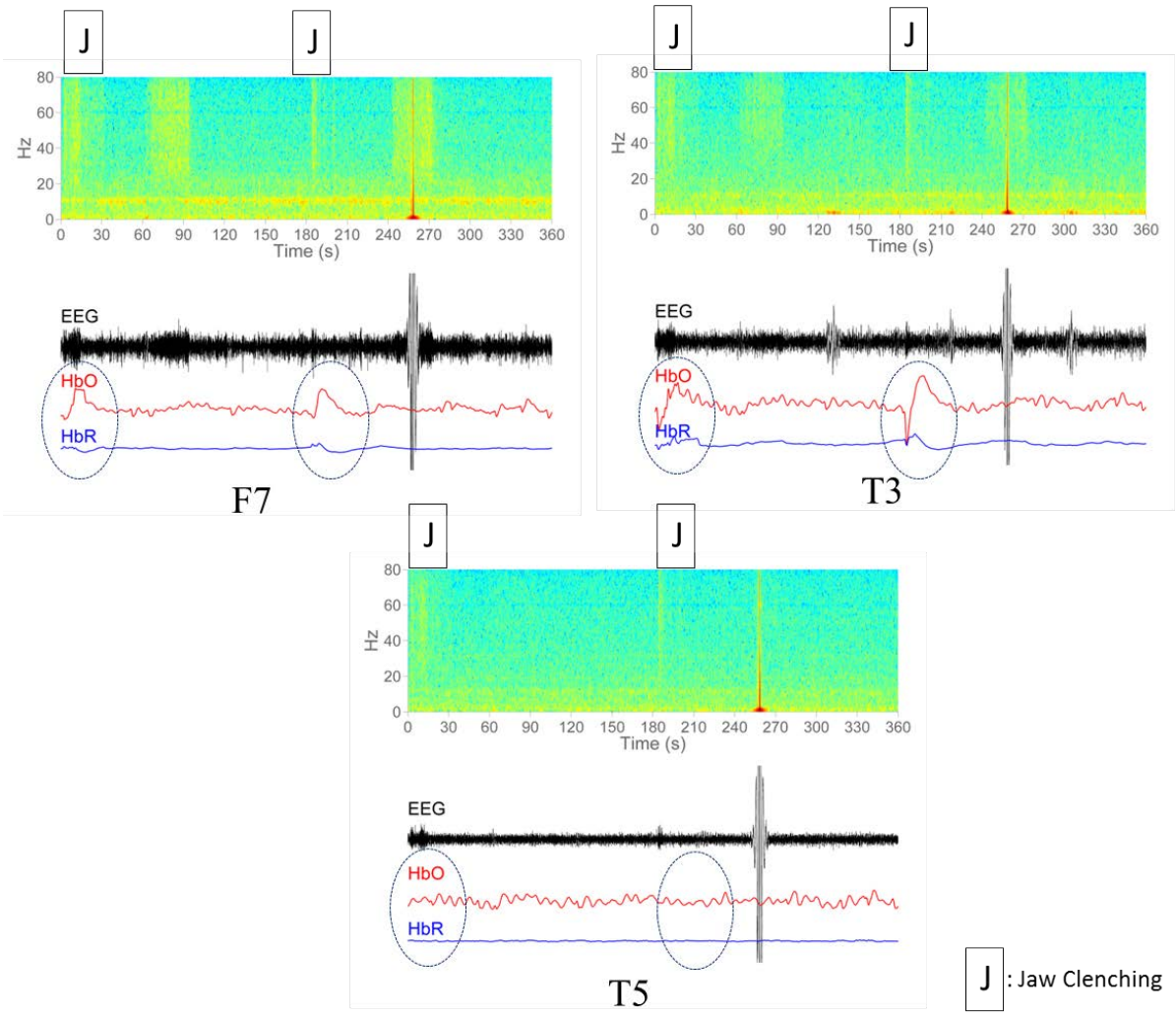

Figure 3.4 EEG spectrogram, EEG signal, and HbO/R concentrations at a different location (F7,T3,T5)

In addition hemodynamic activity is observable for only jaw clenching. Strongest EMG under 200 Hz was generated by smiling. Jaw clenching generated the highest frequency EMG activity (reaching well above 200 Hz) (**Figure 3.5**).

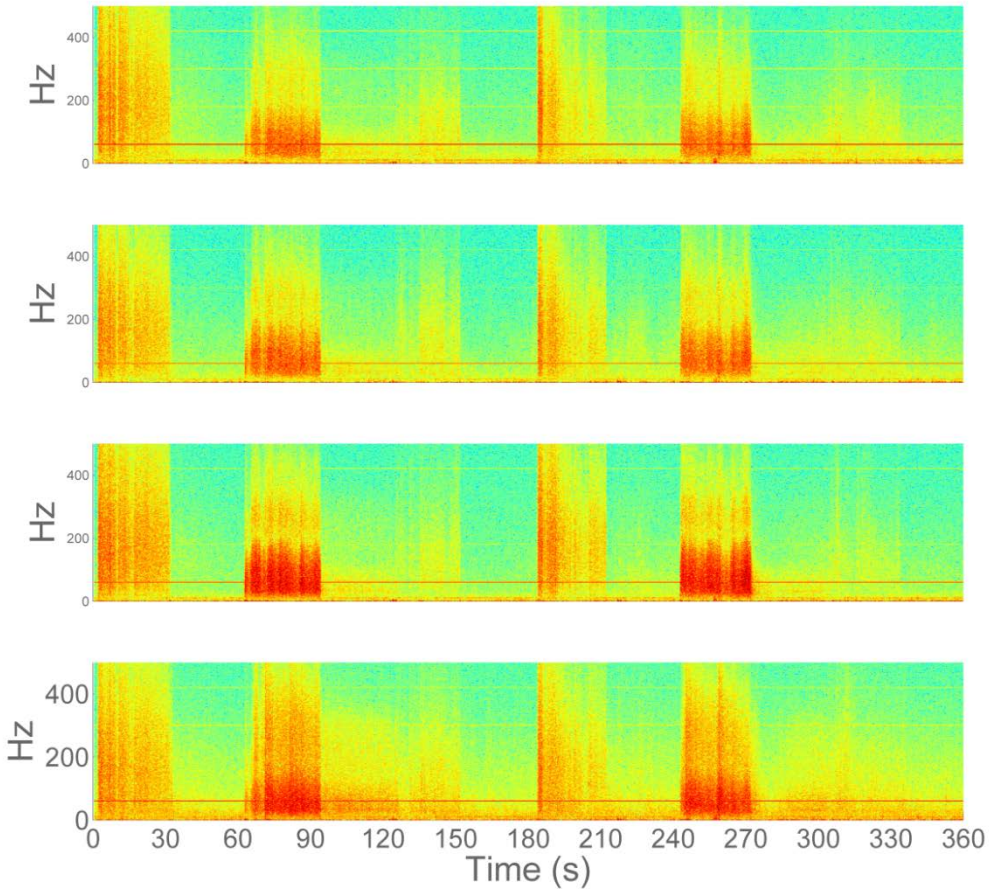

Figure 3.5 Monitoring the effects of artifacts with EEG-EMG-fNIRS.

The temporalis findings that we have made have been elaborated in the second experiment. With this purpose, we measured the neural activity and hemodynamic signals over the whole head with the multimodal imaging system during the only jaw clenching experiment (**Figure 3.6**). The subject was resting with eyes closed and was instructed to clench his jaw twice separated by about 30 s.

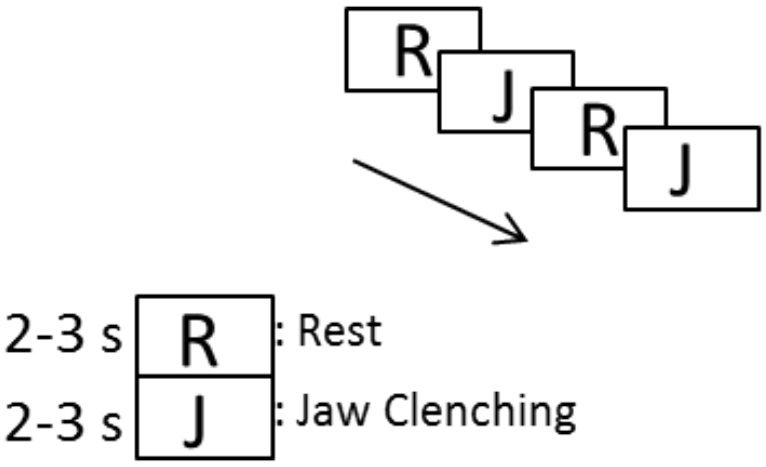

Figure 3.6 Experimental design of jaw clenching artifact experiment

Our spectrogram result shows that the high frequency EMG activity due to the temporalis muscle is picked up by EEG electrodes over a wide spatial scale (**Figure 3.7**). However the corresponding hemodynamic activity is limited to only to those directly over the muscle (F8, T4). The dips in the HbO/R signals that immediately coincide with the rise in EMG are motion artifacts (slight lifting of probes by contracting muscle). Following the EMG with a delay of about 10 s is a strong peak in HbO followed by a negative peak in HbR.

These changes in the Hb concentrations are greater than the magnitude of typical changes due to cortical activity. We can speculate that this magnitude change might be associated with the intramuscular blood flow that decreases immediately after the beginning of the contractions in the temporalis. In simultaneous fNIRS-EEG, temporalis muscle should be considered as a potential EMG artifact which can mask cerebral signals. Time series data for all channels from an experiment are shown in **Figure 3.8.**

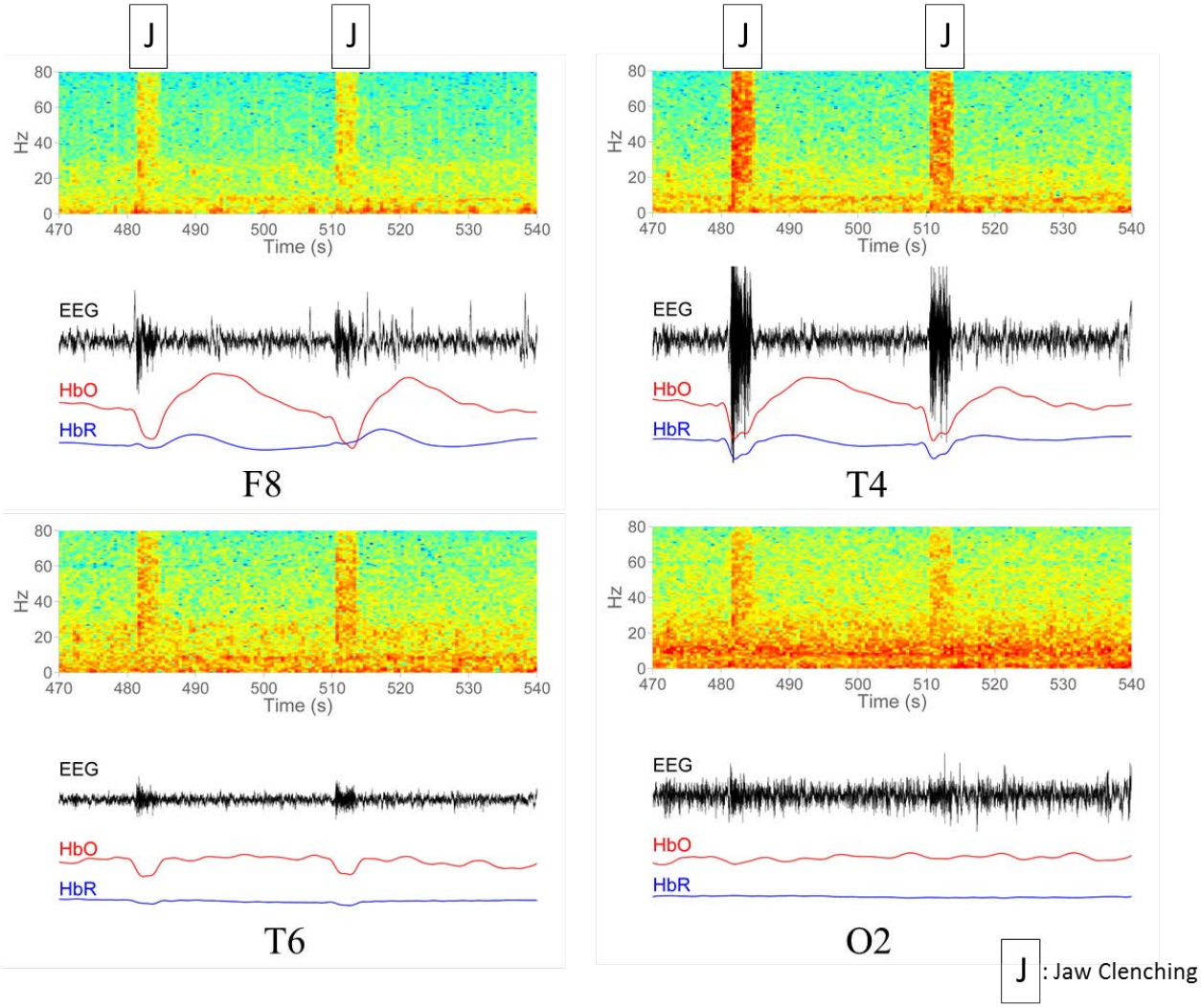

Figure 3.7 EEG spectrogram, EEG signal, and HbO/R concentrations at a different location (T4,T6,F8,O2)

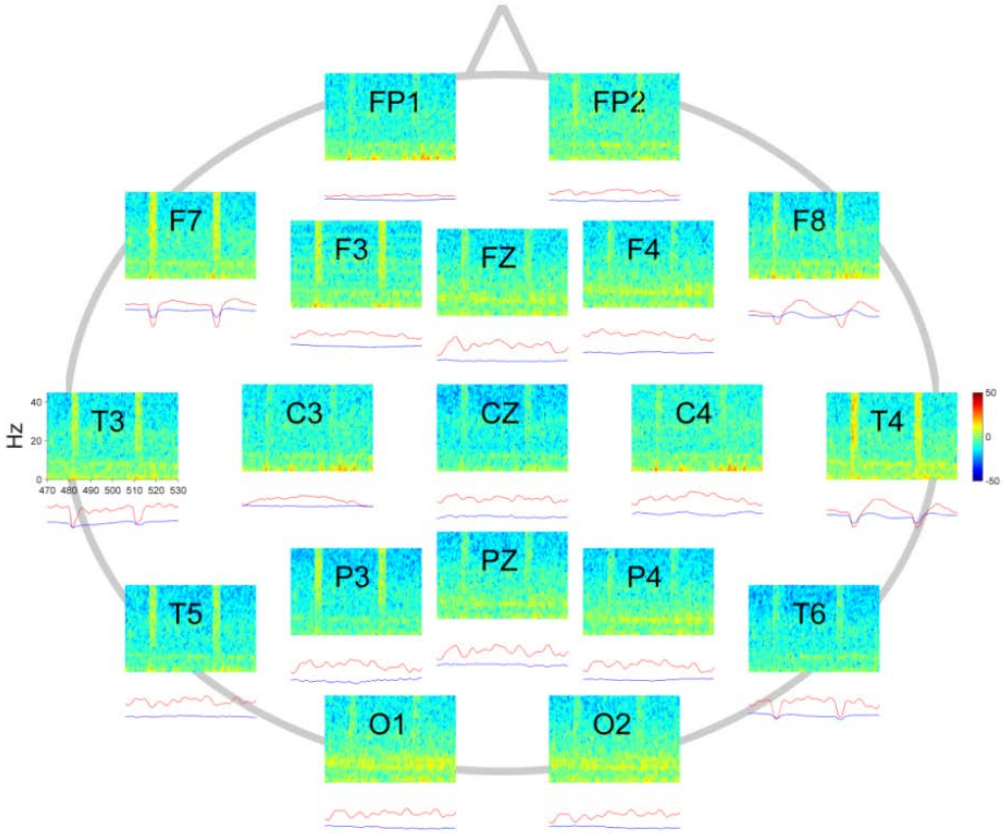

Figure 3.8 EEG spectrogram, EEG signal, and HbO/R concentrations over the whole head.

3.1.3 Validation with Verbal Fluency Task

The verbal fluency (VFT) study was performed on human subjects to test the functionality of simultaneous fNIRS+EEG system. VFT is the one of the most effective tasks for frontal lobe activation. It is a cognitive test that measure subject's ability to retrieve specific information within restricted search parameter. Word search and production requires high cognitive demands. VFT involves several numbers of cognitive components which include searching words, generating target words and recalling. These processes require significant capacity utilization and directly associated to the changes in mental workload. The verbal fluency has been specifically used to show the frontal and temporal lobe activation and cognitive dysfunction (99). Attention and concentration factors that positively affect the performance of the written verbal fluency.

In this experiment, we used the semantical version of the verbal fluency that is the most commonly used task in the fNIRS language studies (100). The activation task was a semantic version of the verbal fluency task (VFT) where responses were either pronounced (VFT-P) or written (VFT-W). Currently, the relationship between neural activity and hemodynamic response during the VFT are under investigation.

The activation task was a semantic version of VFT similar to that described by Schecklmann M. et al., (101). For both VFT-P and VFT-W, a block design was used with six 30s resting periods, three 30s control periods and three 30s activation periods (**Figure 3.9**). During the resting state condition, the subject was instructed to keep her eyes closed and relax without focusing on anything particular while not falling asleep and to stay motionless as much as possible. During the control periods, subjects had to name

weekdays from Monday to Friday. In the first experiment, WFT-P, the subject was instructed to name words from a certain category (animals, fruits and flowers)

In the second experiment, VFT-W, the subject was instructed to write down the words on a white board. During the VFT-W, examiner called categories such as garments, sports and professions. Subjects were responsible to vocalize or write down 8 words (about 3.75 s per word) during each 30 second period for tasks and controls. Four subjects' data are presented.

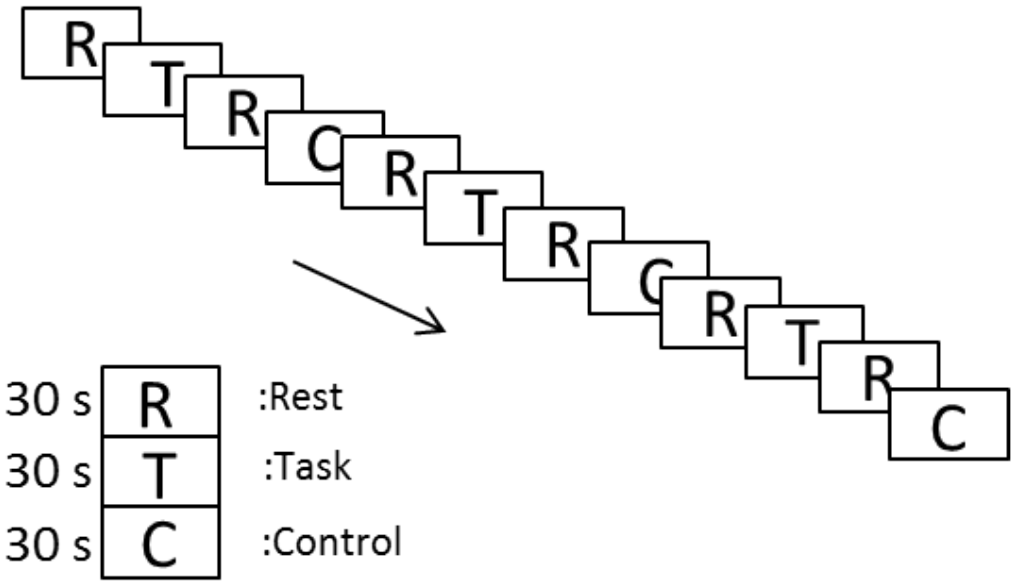

Figure 3.9 Experimental Design of sematic VFT (Task: VFT-W and VFT-P)

Topographic view of synchronized EEG spectrogram and time series of HbO/R concentration changes in the VFT-P have been shown **in Figure 3.10A** and the VFT-W have been shown in **Figure 3.11A.** The 30 second task segments are visible as high frequency EEG in some channels (e.g., FP2, F7). In this experiment**,** EMG was recorded

with the microEEG. The effects of verbal fluency task on muscles are also being monitored. The spectrograms are shown (from top to bottom) of electrodes placed on the subjects Temporalis 1, Temporalis 2, Masseter, and Mentalis in **Figure 3.10B** (VFT-P) and in **Figure 3.11B** (VFT-W). The result showed that pronounced words are visible, especially in high frequency activity on mentalis in the VFT-W. Little or no high frequency EEG activity is seen as compared to the VFT-P. EMG data recorded with the microEEG in the VFT-W showed that little high frequency activity is observed as compared to VFT-P. Based on result in **Figure 3.10** and **Figure 3.11**, we can claim that the VFT-W can be better to use for multimodal imaging as a cognitive task since the noise issues are less than the pronounce The block averaged synchronized fNIRS+EEG in the VFT pronounced and written were computed and shown in **Figure 3.12**, **Figure 3.13** and **Figure 3.14**.

In **Figure 3.12**, the signals have been averaged over the 19 channels and smoothed by using a moving window of size 10 s. The light gray thin curves in the background of each plot show the time series of individual channels in order to show the inter-channel variability. Top row is subject 1 and the bottom row is subject 2. The left column is VFT-P and right column is VFT-W. In each figure the top panel shows the EEG power in the alpha range (13-30 Hz). This range was chosen because it correlated best (by inspection) with the experimental conditions. In the VFT-P tasks the EEG power is obscured by EMG. But the right column shows that when EMG is low as in the VFT-W the beta band power is a good indicator or Rest v Task. Bottom panel shows the concentration changes of HbO (red), HbR (blue), and the CBF (black). HbO signal appears to correlate reasonably well with the experimental conditions.

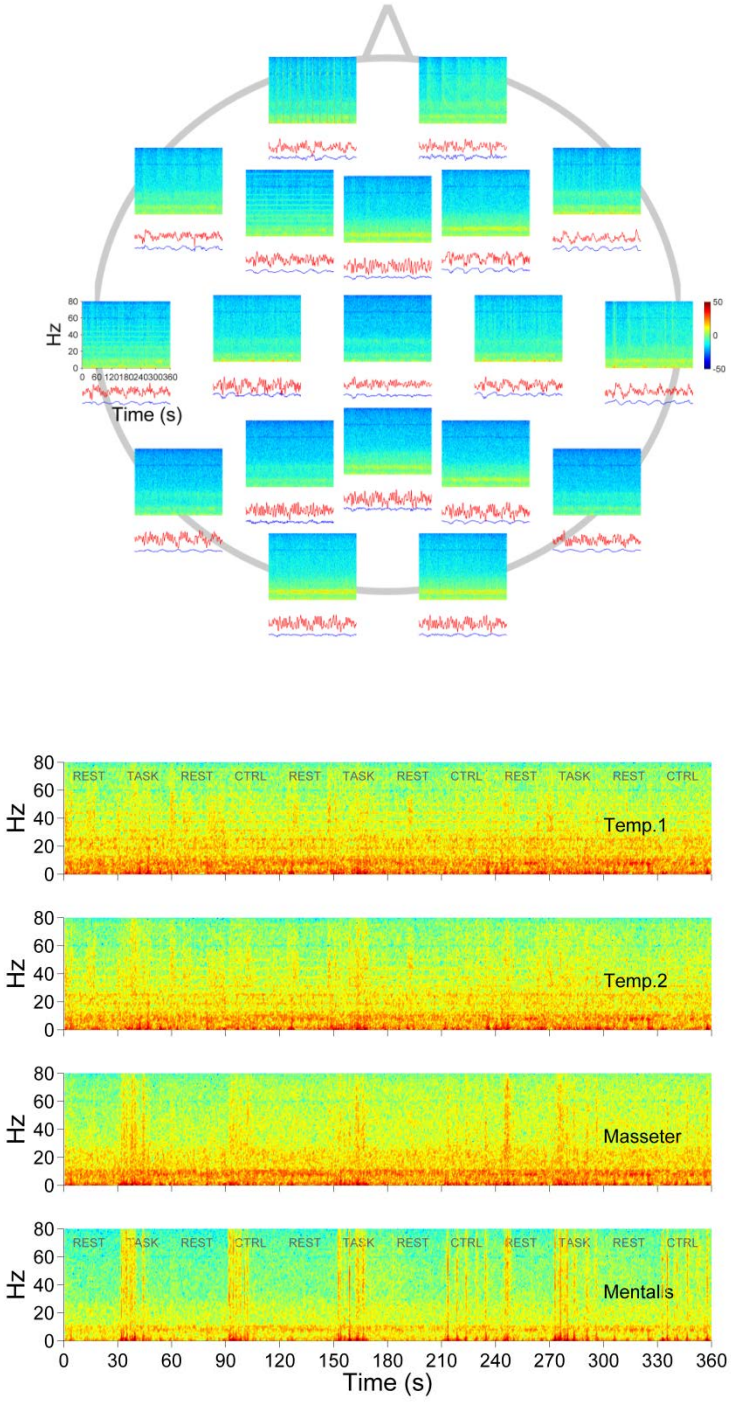

Figure 3.10 Topographic view of synchronized EEG spectrogram and time series of HbO/R concentration changes in the pronounced VFT. EMG recorded with the microEEG

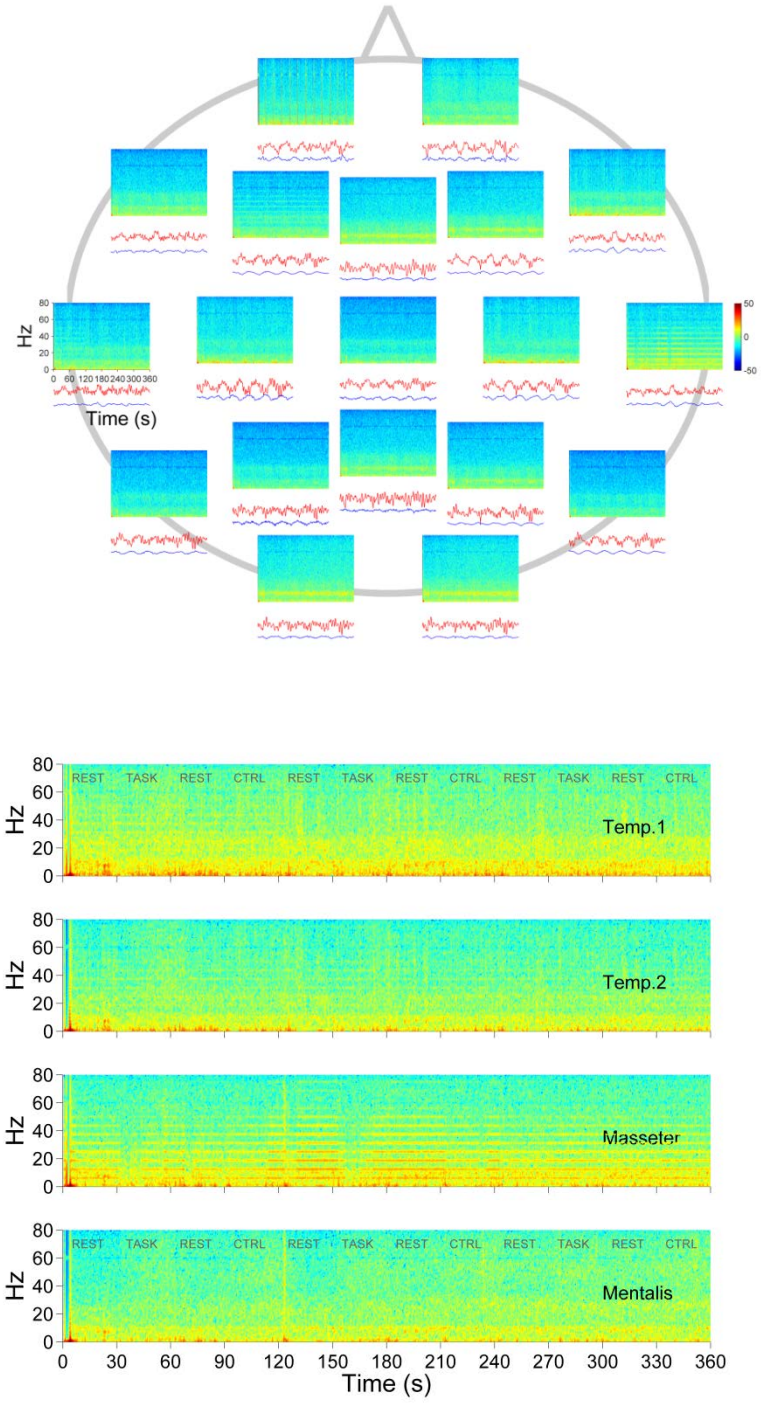

Figure 3.11 Topographic view of synchronized EEG spectrogram and time series of HbO/R concentration changes in the written VFT.

Figure 3.12 indicates that fNIRS in combination with EEG is likely a better predictor of cognitive workload as compared to either modality by itself.

In **Figure 3.13**, the signals are from 4 sensors F7, F8, T3, T4 have been averaged over the channels and smoothed by using a moving window of size 10 s. The light gray thin curves in the background of each plot show the time series of individual channels in order to show the inter-channel variability. The left column is VFT-P and right column is VFT-W. Top panel shows the EEG power in the alpha range (8-12 Hz). Bottom panel shows the concentration changes of HbO (red), HbR (blue), and the CBF (black). These locations were chosen because of their proximity to brain areas most likely to be activated and because their signals varied most with changes from rest to task conditions.

Results show that EEG and NIRS combined are likely to be a better indicator of cognitive task performance than one of these modalities by itself. In the VFT-P the EEG alpha and NIRS signals are poorer indicators of rest-task differences relative to the VFT-W. This is likely due to the masking effect of the EMG and hemodynamic activity from temporalis muscle (e.g., Subject 4). When the EEG alpha signal is a poor discriminator, the NIRS signal may continue to discriminate between rest-task as seen in **Figure 3.13** (Subject 4 VFT-W). These preliminary results showed that there are certain advantages to use multimodality imaging system to distinguish between the absence and presence of cognitive load. Written informed consent was obtained from every subject and the study had been approved by the institutional review board of the University of Houston.

	VFT-P	VFT-W
Subject 1	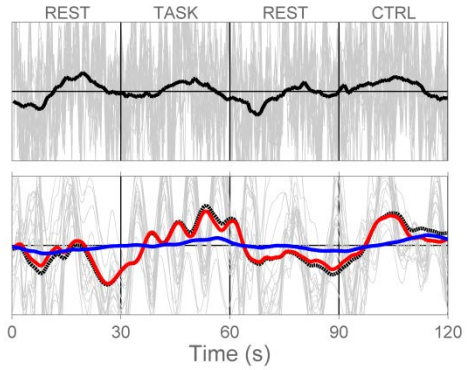	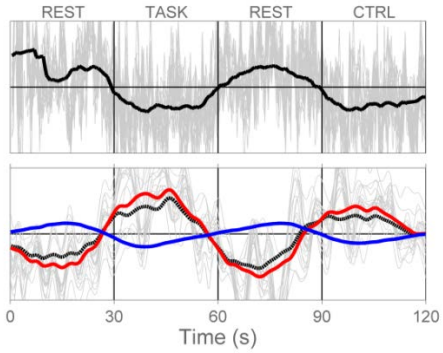
Subject 2	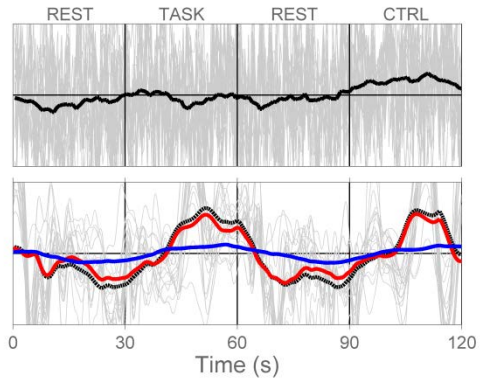	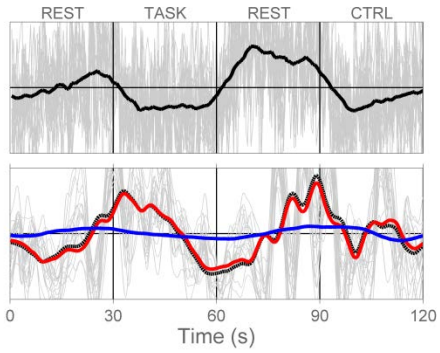

Figure 3.12 Block averaged synchronized EEG-fNIRS in the VFT –P and VFT-W for two subjects for all channels

	VFT-P	VFT-W
Subject 1	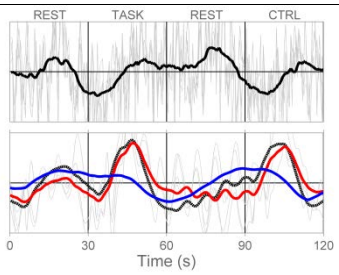	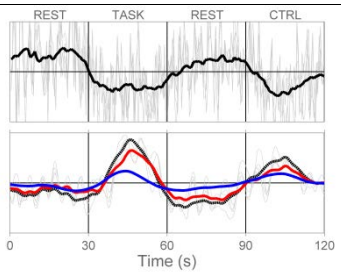
Subject 2	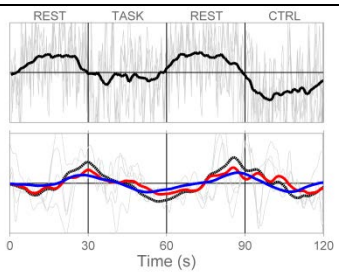	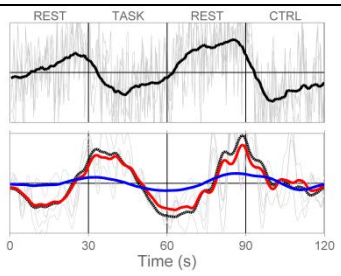
Subject 3	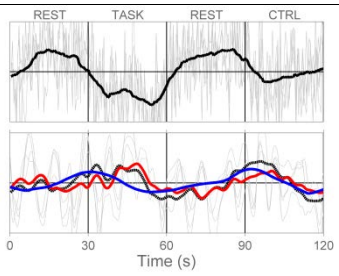	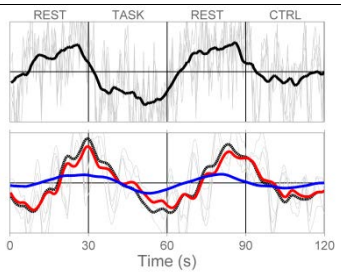
Subject 4	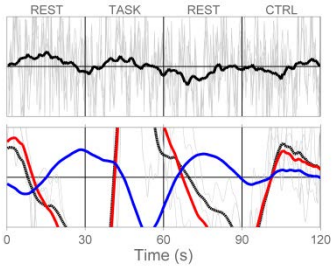	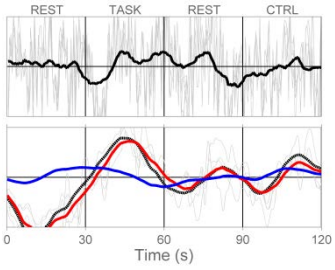

Figure 3.13 Block averaged synchronized EEG-fNIRS in the VFT-P and VFT-W written for four subjects for the average of F7, T3,F8 and T4.

Figure 3.14 corresponds to the top right panel of the previous **Figure 3.13** (Subject 1 VFT-W) but with fewer numbers of selected channels. On the left panel, the signals are the average of F7, T3, F8 and T4. They have also been smoothed by using a moving window of 10 s. Despite the low number of sensors the correlation with experimental conditions apparently did not deteriorate. More remarkably, HbO and HbR are positively correlated for this set of channels. On the right panel, the signals are the average of channels other than F7, T3, F8, and T4. HbO and HbR are negatively correlated for this set of channels. A possible explanation of the difference between the left and right panels is that the areas F7, T3, F8, and T4 experience sufficient increase in CBF so that both HbO and HbR increase despite the conversion of HbO to HbR.

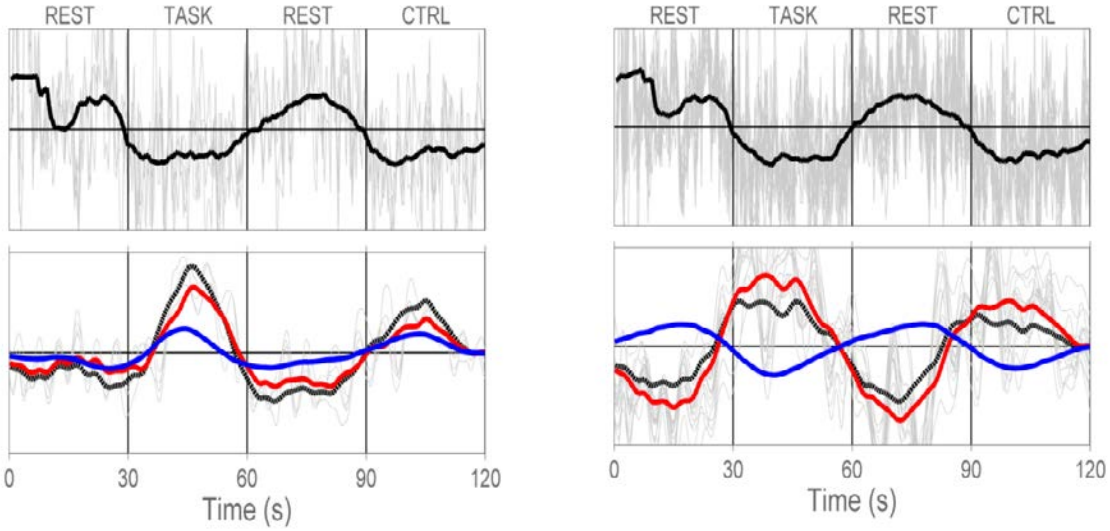

Figure 3.14 Block averaged synchronized EEG-fNIRS in the VFT-P and VFT-W from the **Figure 3.13** (Subject 1 VFT-W)

4 CHAPTER

4.1 Resting Sate Studies with simultaneous fNIRS+EEG

4.1.1 Introduction

In this chapter, simultaneous fNIRS+EEG is applied to the resting state studies. The brains of awake, resting human subjects display spontaneously occurring neural activity patterns whose magnitude is typically many times greater than those triggered by cognitive or perceptual performance. Such resting state (RS) activity is thought to reflect the functional organization of the brain. In addition, both evoked and RS activation affect local cerebral hemodynamic properties through processes collectively referred to as neurovascular coupling. This is a major topic of interest due to its relationship with pathological conditions that include hypertension, stroke, subarachnoid hemorrhage, and traumatic brain injury. Its investigation calls for an ability to track both the neural and vascular aspects of brain function. We used the developed simultaneous fNIRS+EEG system to investigate neurovascular coupling over the whole head during resting states. We used scalp EEG to measure the degree of synchronization of post-synaptic potentials in the brain. Simultaneously we utilized fNIRS to continuously monitor hemoglobin concentration changes in superficial cortical layers. The multi-modal signal from 12 healthy adult subjects allowed us to investigate the association of neural activity in a range of frequencies over the whole-head to local changes in hemoglobin concentrations. Our results verified the delayed alpha (8-16 Hz) modulation of hemodynamics in posterior areas known from the literature. They also indicated equally strong beta (16-31 Hz) modulation of hemodynamics. Signals from the side periphery

were dominated by scalp muscle related activity. Our study aimed to characterize the phenomena related to neurovascular coupling observable by practical, cost-effective, and non-invasive multi-modal techniques.

4.1.2 Study and Experimental Design

Twelve healthy adult volunteers took part in this study (12 male; age mean 26 years (range 24-28 years)). None had a history of psychological illness or substance dependence. Subjects completed informed consent before the experiment and were compensated for their participation. The research was approved by Institutional Review Board at University of Houston. Each subject was seated in a comfortable chair in a silent room with lights dimmed and instructed to relax with eyes closed without exerting any mental effort or falling asleep. The resting state recording lasted 15 minutes.

4.1.3 Analysis

The EEG signals were preprocessed by bandpass filtering 0.5 - 70 Hz and optical signals at 0.01 - 0.5 Hz. For each channel the power spectrogram of the EEG was computed using a 1.2 s Hamming window with 50% overlap. The EEG power and optical time series were then resampled at 2 Hz. From the NIRS raw signals the concentration of HbO and HbR were computed using the Modified-Beer-Lambert-Law (54). We verified that changing the spectrogram time window size and the global resample rate within a wide range had no effect on our results. The parallel recording of neural activity and hemodynamics allows the application of system identification techniques to generate a model of the response mechanism. We built an elementary model by computing the

hemodynamic impulse response to the neural activity. The synchronized EEG power and Hb signals were used in a correlation analysis. We computed the delayed correlation of the EEG frequency band power with the Hb signal as the covariance of the two signals divided by the product of their standard deviations. The autocorrelation of the EEG power as a function of frequency and time difference was sharply peaked at zero differences and closely approximated a two dimensional Dirac delta function, as verified by our subject-averaged data an example of which at 10 Hz is shown in **Figure 4.1** (other frequencies gave similar peaks, not shown). Approximating the autocorrelation as a delta function, the impulse response at each frequency was the cross covariance function of the EEG power and Hb concentration changes.

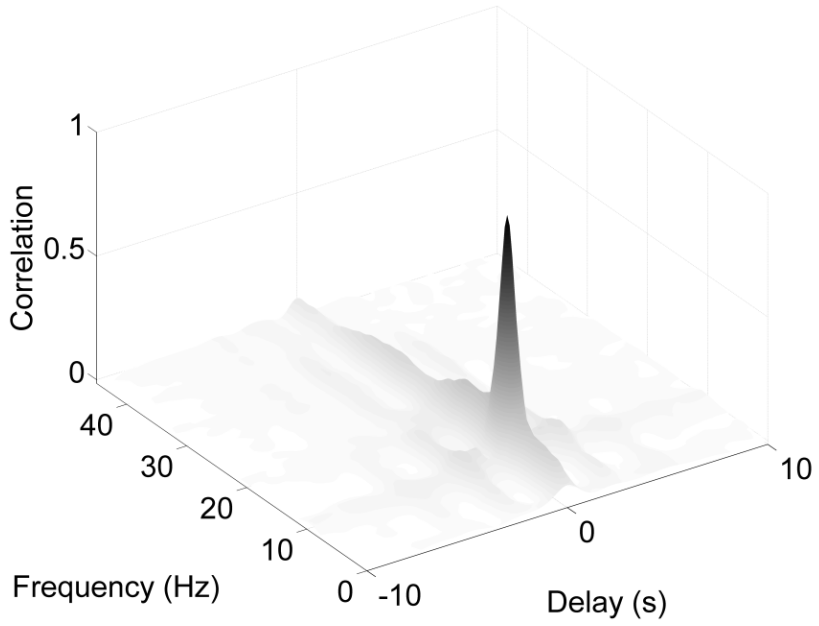

Figure 4.1 The frequency and delay dependence of the autocorrelation of EEG power

The EEG power in the frequency band f at time t is denoted $p(f,t)$. The hemoglobin concentration change $h(t)$ is given as the integral over all relevant frequencies of the

convolution of EEG power with the frequency dependent impulse response $R(f,\tau)$ where τ is the time delay:

$$h(t) = \int df \int_0^\infty d\tau' R(f,\tau')\, p(f, t-\tau'). \quad \text{(3-a)}$$

Inserting the above equation into the definition of the cross covariance

$$c(f,\tau) = \langle\, p(f,t) h(t+\tau) \,\rangle\,, \quad \text{(3-b)}$$

where $\langle \cdot \rangle$ denotes time average, yields

$$c(f,\tau) = \int df' \int_0^\infty d\tau'\; R(f',\tau')\;\; a(f', f, \tau-\tau')\;\;, \quad \text{(3-c)}$$

where $a(f', f, \tau-\tau')$ is the two dimensional autocorrelation of the EEG power. An example of the autocorrelation at $f = 10$ Hz calculated from our data and subject averaged is given in Figure 3. This supports the assumption that the autocorrelation can be approximated as a two dimensional delta function. Inserting $a(f', f, \tau-\tau') = \delta(f'-f)\,\delta(\,\tau-\tau')$ into the above equation yields $R(f,\tau) = c(f,\tau)$. i.e. that the cross covariance equals the hemodynamic impulse response.

Statistical Analysis

We used the cross covariance of EEG power with the Hb concentration changes obtained from the 15 minute experimental data as an estimator of the hemodynamic impulse response. In order to use this estimator we needed to evaluate its baseline variability. We achieved this by computing the cross covariance of EEG power with Hb concentration changes where the EEG and fNIRS data were taken from two separate experiments. Since the neural activity fluctuations in a RS experiment cannot systematically associate with the Hb changes in another one, the resulting values only indicate the noise baseline of the cross covariance estimator. For a set of N experiments

there were $N(N-1)$ pairs of distinct experiments that helped create a large baseline reference set. The distribution of cross covariance values was highly non-Gaussian (kurtosis=3.76). We used this reference set and the Kolmogorov-Smirnov test in order to determine the statistical significance of the impulse response.

4.1.4 Result

An example of the preprocessed data from one resting state experiment is shown in **Figure 4.2**. The figure shows a 2 minute segment selected because it illustrates several of the features frequently encountered. Noteworthy are the dominant posterior alpha rhythm at approximately 10 Hz particularly strong in the ocular and parietal channels but visible almost globally. The figure also illustrates the spontaneous fluctuations in the amplitude of the alpha oscillation. Closely examining the spectrogram in F7 shows higher power in narrow ranges at multiples of the NIRS sample rate 6.25 Hz. This is an example of an artifact created by a NIRS source cable when it is close to an EEG lead and eliminated by rearrangement of the cables. The EEG spectrogram occasionally reveals muscle artifacts in the gamma range although none appears in this example. Another noteworthy feature in **Figure 4.2** is that the HbO concentration changes (red curve) appears to surge in the frontal and temporal channels F7, F8, T3, and T4 toward the end of the time segment shown, returning to baseline after about 20 s. The HbR concentration change (blue) during the same period undergoes dip smaller in amplitude and delayed with respect to the HbO. We verified in separate experiments (not shown) that this pattern is activated when the subject clenches her jaw contracting the temporalis muscle located directly

under those channels. The amplitude of these concentration changes is greater than any changes driven by cortical activity and therefore easily recognizable.

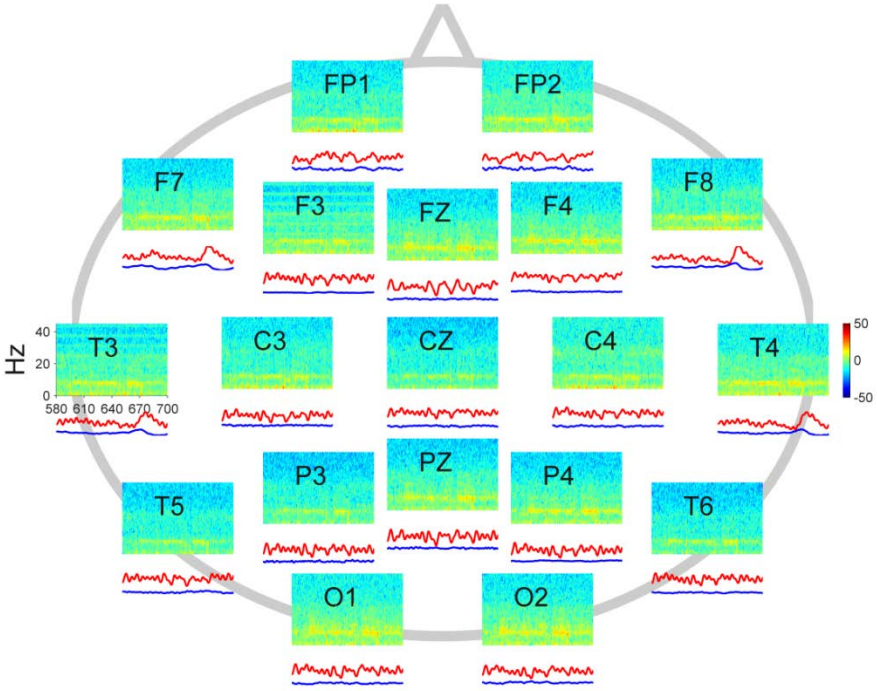

Figure 4.2 Example of whole head EEG spectrogram and HbO (red) / HbR (blue) time series from a representative subject 3.

Figure 4.3 shows the wholehead delayed correlations between the EEG spectrogram and the HbO (left) and HbR (right) changes from the experiment shown in **Figure 4.2**. The channels susceptible to being affected by facial muscle oxygenation, F7, F8, T3, and T4, show that the HbO typically increases 10 s after an increase in EEG power particularly in the beta range. The remaining channels, with possible differences in the frontopolar (FP) channels, have a pronounced negative correlation between the EEG power in the alpha range and HbO changes with an approximate 8 s delay. There is a similar but less strong relationship with the beta power. The correlation of HbR changes

with EEG power shows a similar pattern but with an opposite sign, later onset, and longer duration.

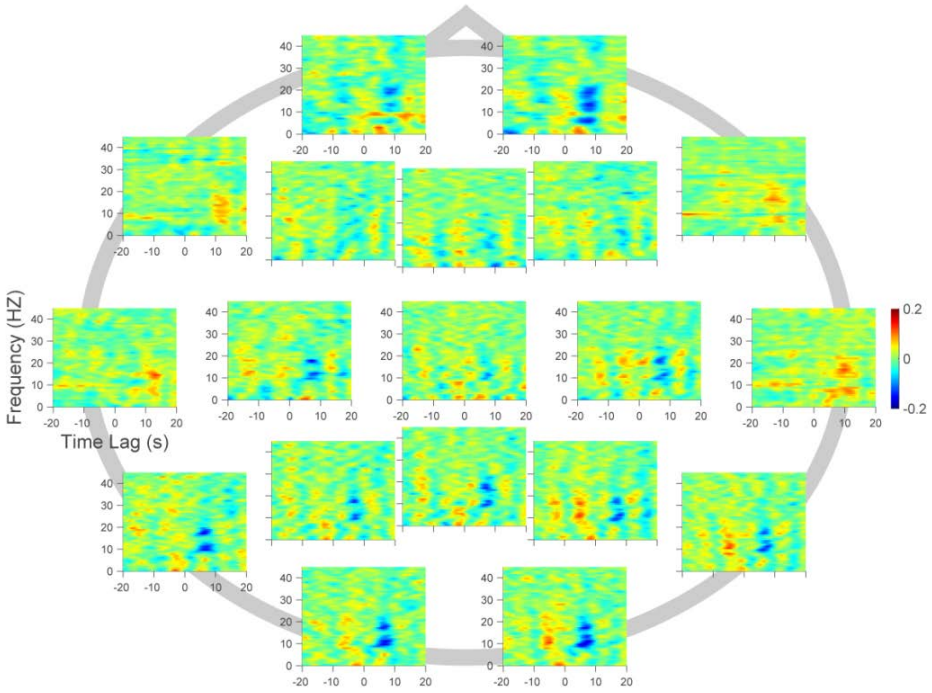

Figure 4.3 One subject wholehead delayed correlations.

In order to show the range of inter-subject variability we present, in **Figure 4.4**, the delayed correlations (for HbO only) for all 12 experiments in this study. Some of the inter-subject variability was as follows. In the subject in the top row, second column, the delayed negative correlation in the alpha band in posterior areas was accompanied by another peak with the opposite sign at the nearby theta band with a similar delay. In the subject in the middle row, first column, the strongest negative correlation occurred in the beta band. In the subject number 5, the negative correlation appeared to be distributed

equally in the alpha and beta bands and had an earlier onset. Despite such inter-subject variability, however, the most salient feature shared by most subjects was a negative correlation between the EEG power, particularly in the alpha and beta frequency ranges, and the HbO concentration changes with a delay at approximately 8 s. This appeared most strongly in the parietal and occipital areas but was also approximately replicated by the frontopolar region.

The strong positive correlation with gamma power observed in some subjects (e.g., middle row, last column) in channels T3, T4, F7, F8 was due to contamination from the scalp muscles. In these cases there was also a pattern of zero-lag correlation distributed across higher frequencies. This was attributable to a motion artifact introduced by the flexing of temporalis muscle that simultaneously affects the EEG and NIRS probes. We verified the muscle origin of these features in a further experiment described below.

We averaged all the correlations shown in **Figure 4.5** in order to reveal common patterns among them and minimize the variable part of the correlation. **Figure 4.5** clearly shows that the 8 s delayed inverse correlation of HbO with EEG alpha and beta power are the salient common feature of our results in most channels. This is replaced by the positive correlation with a similar delay in the channels corresponding to the temporalis muscle. The corresponding correlation of HbR presents a similar pattern with the opposite sign and later onset.

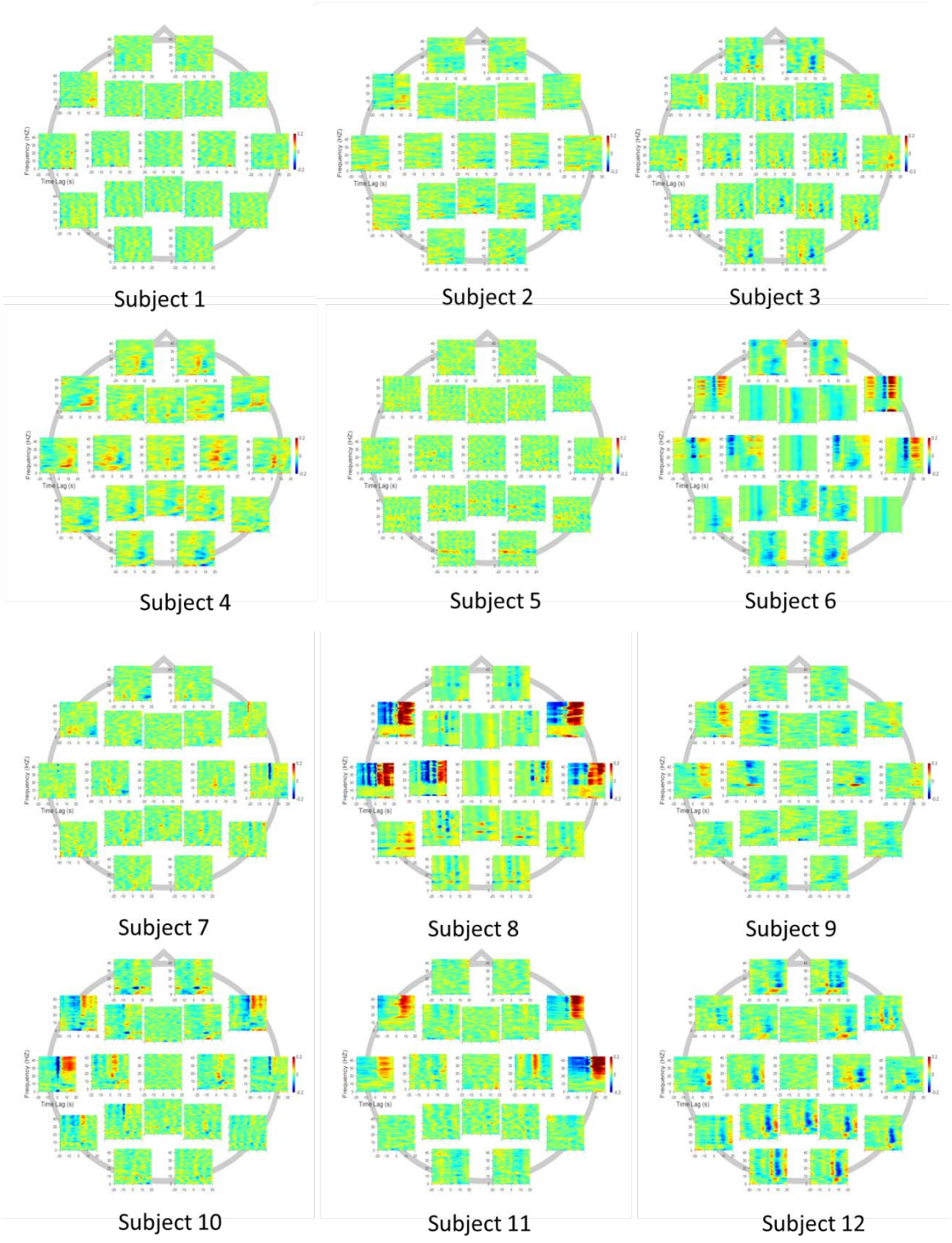

Figure 4.4 Whole head time delayed correlation maps between EEG power and Hbo changes for 12 subjects.

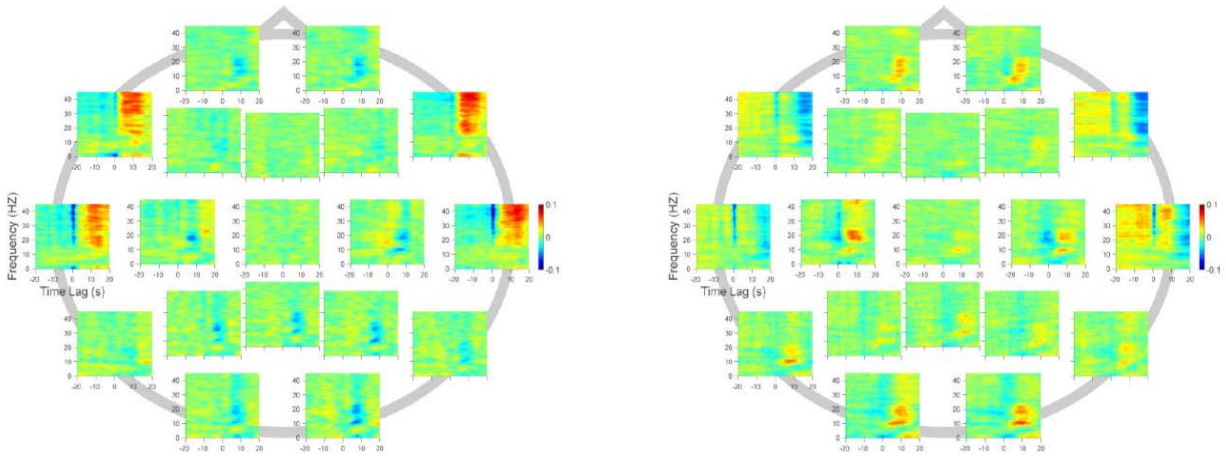

Figure 4.5 Subjects averaged delayed correlation between EEG power and HbO (left) and HbR (right) concentration changes

Figure 4.6 and **Figure 4.7** describe the modulation of hemodynamics by individual EEG frequency bands over three distinct regions. The mean correlation (thick curve) and one standard deviation region (shaded) of the group of 12 subjects are shown. The rows 1-3 represent, respectively, the frontopolar region (average of channels FP1, FP2), the side periphery (F7, F8, T3, T4), and the occipital and parietal regions (O1, O2, P3, PZ, P4). For each value of the delay we tested the null hypothesis that the group of values of the correlation had the same distribution as the baseline reference set constructed as described in Methods. The delays marked with a single asterix indicate $p \leq 0.005$ and those marked with a double asterix indicate $p \leq 0.001$ level of significance computed according to the the Kolmogorov-Smirnov test. The figure indicates that the strongest coupling occurred in the alpha and beta band in the occipital and parietal regions and at the side periphery. The latter was of muscular origin and was accompanied by a sharp feature at zero-lag due to motion artifact.

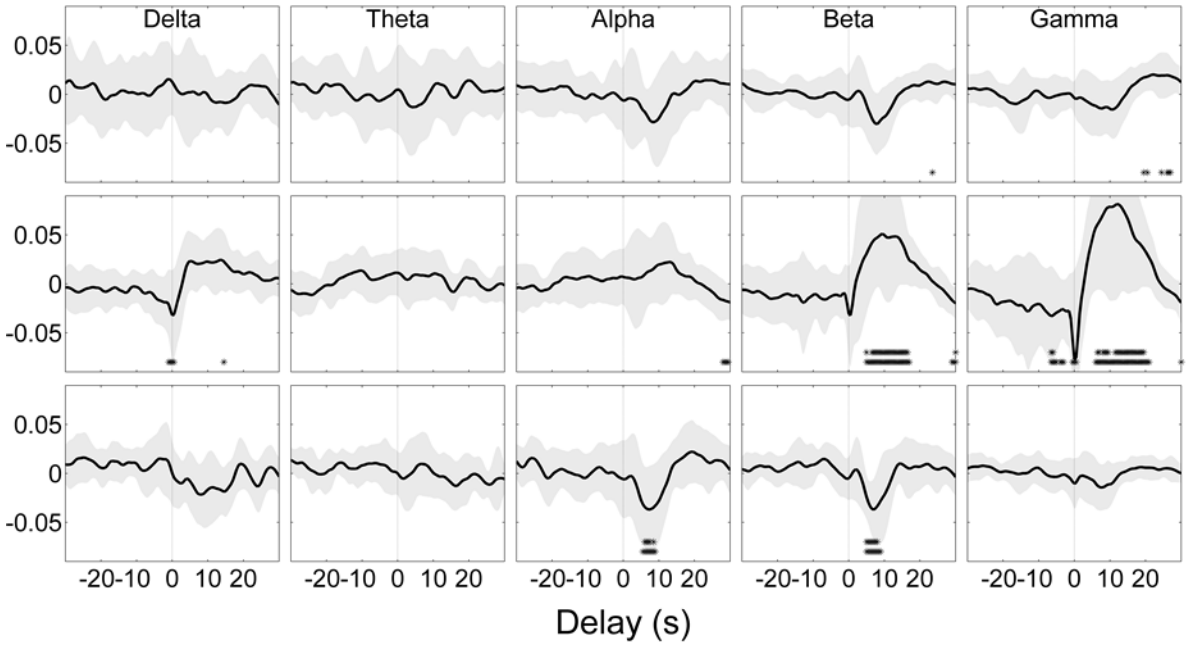

Figure 4.6 Regionally segregated and subject averaged delayed correlation between EEG frequency band power and HbO concentration changes. Single asterix indicates $p \leq 0.005$ and double asterix indicates $p \leq 0.001$

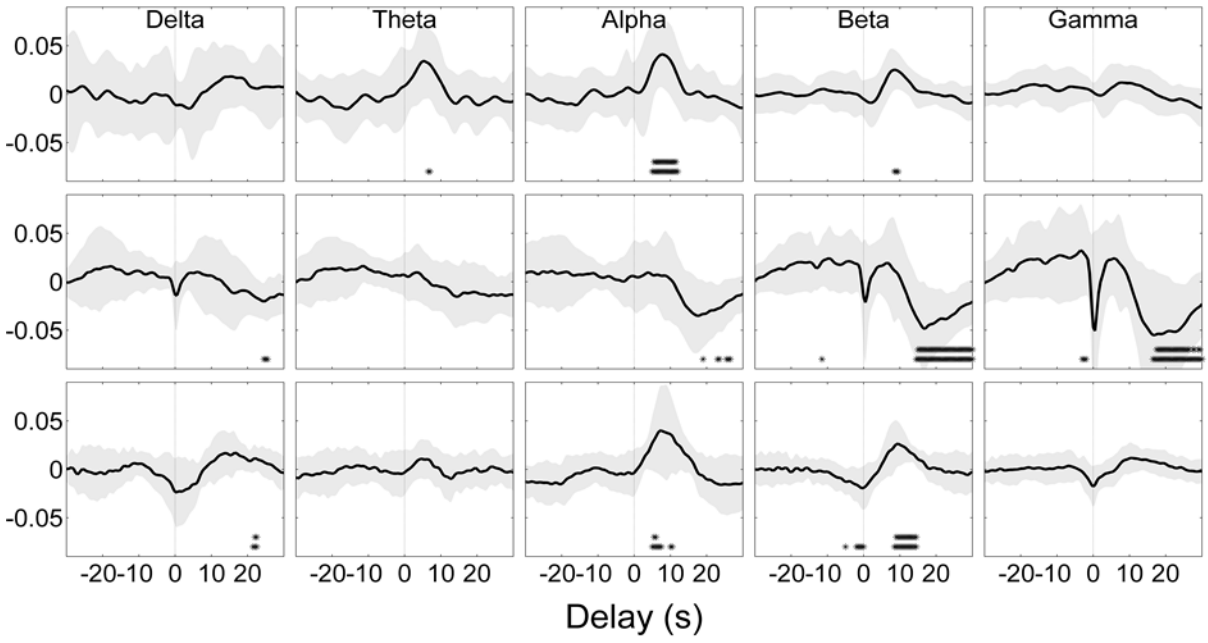

Figure 4.7 Same calculation as in **Figure 4.6** but for HbR. Single asterix indicates $p \leq 0.005$ and double asterix indicates $p \leq 0.001$

The corresponding delayed correlations for HbR shown in **Figure 4.7** had similar features but the peaks were negative, wider, and delayed by several seconds. This was consistent with the time course of HbR relative to HbO observable in **Figure 4.2.** EEG theta power appeared to significantly modulate HbR, a feature that was absent from **Figure 4.7**. For 12 subjects, a quantitative investigation of delayed correlations is shown in **Table 4.1**.

Table 4.1 Subject specific characteristics of the delayed correlation between EEG alpha power and the hemoglobin concentration changes

SUBJECT	HbO		HbR	
	Peak Value	Time Delay of the Peak Value (seconds)	Peak Value	Time Delay of the Peak Value (seconds)
1	0.044	6.5	-0.017	7.5
2	-0.041	5.5	0.053	6.5
3	-0.09	7.5	0.109	8.5
4	-0.058	6.5	0.123	8.5
5	-0.011	5.5	0.017	10.5
6	-0.069	4.5	0.05	8
7	0.03	4.5	0.021	5
8	-0.045	7	0.013	7
9	-0.023	6	0.017	10.5
10	-0.085	4.5	0.064	4.5
11	-0.049	8.5	0.037	9
12	-0.136	9.5	0.024	7

Our results (**Figure 4.8**) indicate that delayed correlation of EEG power with BOLD found in fMRI studies is replicated by fNIRS+NIRS. The horizontal axis shows the time delay in **Figure 4.8**

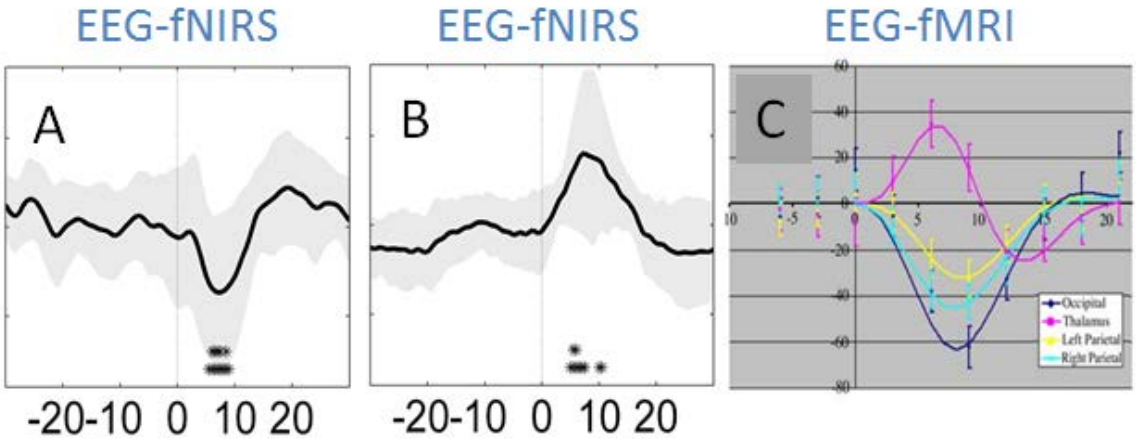

Figure 4.8 Coupling of EEG Alpha power with hemodynamics by delayed correlation in resting healthy subjects. Comparison between EEG+FNIRS and EEG+FMRI results. (A) HBO. (B) HBR. (C) EEG-fMRI result from de Munck et al., (92)

4.1.5 Discussion and Conclusion

The alpha modulation of brain hemodynamics was known from numerous previous studies (22, 28, 41, 93, 102, 103). Our study is the first, to our knowledge, to examine the EEG full-spectrum power modulation of hemodynamics by fNIRS+EEG over the whole-head. We found significant modulation of Hb concentration changes by beta power and also significant modulation of HbR by theta activity in frontopolar regions. We also confirmed that the hemodynamic response function generally contains a delay at approximately 8 s.

de Munck et al., (92) and Goncalves et al., (22) found that a minority of their subjects had delayed alpha hemodynamic responses whose sign was reversed relative to the group average. Similarly, one of our 12 subjects showed a small positive correlation between HbO and EEG alpha at about 8 s (**Figure 4.4**), which was the opposite of the group average. One possible explanation for such variability is intersubject differences in hemodynamics. Another possibility is that hemodynamic response is non-stationary and

the data we have collected were confounded by unknown state changes in RS. For example a subject briefly falling into light sleep during RS is not uncommon. Further experiments with a larger data set are needed to distinguish between these hypotheses.

Our results indicate that RS transient increases in neuronal synchronization in the alpha or beta frequencies (as indicated by a rise in EEG power in these bands) are typically followed by a decline in the oxygenated hemoglobin concentration. HbO is closely related to local cerebral blood flow (CBF), naturally leading to the conclusion that higher power in these bands correlates with lower metabolic demand. This may appear paradoxical given that higher EEG power arises from elevated synaptic activity and synaptic activity is known to dominate metabolic demand (12). However note that the transition to synchronization by a neuronal population may come about through diverse paths including changes in input, synaptic gain, and axonal delay (104). One such transition involves a decrease in the input to a population. Assuming that the synchronization in question follows this path (supported by the fact that alpha appears when the eyes are closed) then it would naturally be accompanied by a decrease in metabolic demand. Hence although the generation of the rhythm requires energy the net effect of increase in its power may well be a metabolic decrease and a decrease in local CBF. Our finding of anticipatory hemodynamic signal in a small subset of subjects was consistent with what is known from animal studies (105). The appearance of anticipatory hemodynamics may be due to neural activity that is not picked up by scalp EEG. If this proves to be the case then it may be utilized in detecting patterns missed by scalp EEG.

Does the pervasive ~8 s hemodynamic delay have a functional significance? It may well be an inevitable consequence of the structural properties of vasculature such as

microvessel elasticity or the characteristic activation time of vasoactive agents. Simultaneous intracranial electrocorticography and fMRI has indicated that a tight relationship exists between BOLD signal and broadband gamma in humans (106, 107) and animals (76, 108). In our study the delayed negative correlation of EEG alpha and beta power with HbO was topographically widely distributed but absent at the side periphery where it was replaced the gamma modulation of Hb due to scalp muscle. In order to investigate if the muscle oxygenation was masking an underlying pattern we repeated the calculations in **Figure 4.6** and **Figure 4.7** using only the 3 subjects who by inspection did not have gamma correlations. The results (not shown) contained no significant modulation of hemodynamics by gamma in any region.

The main limitation of our investigation was that the spatial resolution of EEG was low so that the local neuronal input to the hemodynamics is not well resolved. This may account for the observed lack of significant associations with hemodynamics in delta and gamma bands. Another reason for this may be that such associations with scalp EEG were weak and the amount of data we collected did not enable them to achieve statistical significance. The results in dramatically illustrated the fundamentally higher space resolution of fNIRS: the high frequency EEG activity associated with jaw clenching was observed distributed over a wide area whereas the corresponding NIRS signal was confined to the location of the muscles. Future studies that include EEG source reconstruction and quantitative modeling of the hemodynamic response constrained by data (63) will be helpful in overcoming these limitations. Based on existing literature we expected to find a significant modulation of hemodynamics by alpha rhythms in the posterior cortex but we wished to extend the investigation to the whole-head and full

spectrum of EEG. In this study we verified the well-known delayed alpha modulation of hemodynamics in posterior areas. We found an equally strong beta power modulation of hemodynamics. We also found a statistically significant theta modulation of HbR concentration in frontopolar regions. Signals from the side periphery were dominated by muscle electrical and oxygenation activity. Our results indicate that whole-head fNIRS+EEG recordings are able to detect diverse patterns of neurovascular coupling over a range of frequencies of neural activity.

5 CHAPTER

5.1 General Discussion and Future Work

Simultaneous investigation of the neural activity and hemodynamic changes is important to better understand neurovascular coupling in humans. fNIRS+EEG has significant advantages compared to fMRI+EEG. fNIRS is an affordable technology that provides signals that are closely related to the BOLD signal provided by fMRI. Our results and other studies (35, 93) indicate that delayed correlation of EEG power with BOLD found in fMRI studies is replicated by fNIRS+EEG

In this study, triplet holders distributed over the whole head at standard 10-20 locations are able to measure simultaneous fNIRS-EEG from human head. As expected fNIRS is able to localize activity far more than EEG is able to. Artifacts occur in the form of contamination of EEG signal by the power modulation of fNIRS sources and from the electrical/hemodynamic events in facial muscles, particularly temporalis. Although artifacts exist they do not significantly decrease the system's usefulness for tracking cortical states.

There is a significant and consistent time-lagged correlation between the alpha power of neural activity and the HbO/HbR concentrations particularly over the occipital and parietal areas. This is consistent with findings of previous EEG-fMRI studies and holds promise for practical, bed-side diagnosis and monitoring of Alzheimer’s disease, major depressive disorders and ischemic stroke. Our results showed that the multimodal imaging system is a powerful tool to study the relationship between neural activity and hemodynamic response.

Overall, this thesis describes a first step towards the investigation of neurovascular coupling with simultaneous fNIRS+EEG over the whole head. The developed system offers significant advantages and many are yet to be fully exploited. More advances are required, particularly in terms of developing the new system with high density optodes arrangement and new data integration methods. High-density arrangements will enable us to produce 3D images (optical tomography) from the cortex.

Our experiments showed that the simultaneous fNIRS+EEG is a promising tool for the investigation of neurovascular coupling. We still need to explore more the patterns of correlation between EEG power at different frequencies and hemodynamic response. Currently, there are no fundamental problems to simultaneous fNIRS+EEG becoming a routine neuroimaging technique, for both research and clinical applications.

This thesis can serve as a foundation for future work, which may focus on clinical measures and quantitative features extracted from the simultaneous EEG+NIRS signals Firstly, it may help motivate development of a portable, wireless simultaneous fNIRS+EEG system. This portable system can be applied in a clinical and resource limited settings. Two potential application areas will be discussed. Next section will discuss why fNIRS+EEG may prove to be of great utility in the study of traumatic brain injury. In addition, the measurement of mental load will be discussed.

5.1.1 Portable fNIRS+EEG with TBI

A potential future application is to design and develop a practical, wearable, and whole-head integrated simultaneous EEG and fNIRS brain imaging and data analysis system for early discrimination of the long term effects of mild traumatic brain injury.

In a report to Congress of the United States by the Center of Disease Control (CDC), the mild traumatic brain injury (mTBI) accounts for at least 75% of all TBI, with magnitude and impact of which are underestimated by current surveillance systems. The report also pointed out that more than 1.5 million people experience mTBI each year in the US, at a cost of nearly $17 billion each year. In the army, the risk is even higher with about 28,000 service members with TBI each year (115,116). Those personnel who sustain a second concussion before the adequate treatment of the previous mTBI can lead to long-term neuronal injury. The Defense Centers of Excellence have looked into innovations for such portable device with field deployable that may be able to detect mTBI early after injury.

mTBI is one of the most common neurological disorders with a broad spectrum of symptoms and morbidities. Because the symptoms may not be present or noticed at the time of injury, they are often missed by the injured person, family and doctors. Currently, there is no objective diagnostic or prognostic measure of mTBI that can be widely used for outpatients at an affordable cost with easy setup. The impact to the patient and the family can be devastating. The current protocol requires hospitalizing the patients, testing using expensive and complicated medical devices like X-ray, computed tomography (CT), MRI (magnetic resonance imaging) and single-photon emission computed tomography (SPECT) or simply self-reports.

There are no clear EEG features that uniquely correlate with mTBI, and EEG abnormalities are far more common than clinical symptoms in the initial months following injury. Thus EEG in mTBI is beset by very low specificity. fMRI based measures have been shown to provide markers of mTBI with relatively high sensitivity

and specificity. However fMRI is impractical for most settings due to its size, expense, and unsuitability for some subjects such as children. fNIRS, on the other hand, is a light-weight, affordable technology that measures local hemoglobin concentration changes that are closely related to the blood oxygen level dependent (BOLD) signal of fMRI. The interpretation of EEG can be improved and EEG data compressed by using NIRS as statistical priors. The quantitative whole-head monitoring investigation of neurovascular coupling is critical for eliciting measures related to mTBI because of implications of this disease for reduced cerebral perfusion, decreased capillary diameter, and higher reactivity of blood vessel smooth muscles.

5.1.2 Simultaneous fNIRS-EEG in mental workload measurement

Simultaneous fNIRS+EEG can be used for investigating the mental workload. Human information processing model in cognitive science is a reasonable foundation for understanding mental workload. This model proposes that human cognition (which concurrently involves processing of perceptual input and use of working memory) has a limited capacity. This capacity is increased during learning when different entities can be conceptually grouped under schemata, reducing the number of disparate items to be processed and decreasing the load. This explains why increasing expertise is related to automating skills and reduces mental workload (109).

The model also explains why secondary task performance can be used as a measure of mental workload, since lower workload implies higher excess processing capacity. Fatigue lowers the amount of resources available for processing and contributes to higher mental workload. Evidence indicates that minimally invasive operations are more

workload intensive than open operations. In addition, a trainee who achieves expert level on the surgery simulator may show lower performance in OR and the amount of performance decrement correlates with mental workload during training (110).

A vast body of literature demonstrates that human scalp EEG can help track mental states such as arousal, sleep, alertness, and cognitive function (19). However the application of EEG for measuring surgeon mental workload is rare. Guru et al., (111) describes the correlation between a set of EEG measures and performance of individual surgeons during simulated robotic surgery. To date, the EEG simultaneously recorded from a surgical *team* and its relationship to a wide range of OR procedures have not been investigated. This is likely due to the fact that EEG has been difficult to use outside of its traditional roles in the neurology clinic. A platform based on fNIRS+EEG can use miniature, wireless sensors that allow high quality, unobtrusive recording from surgical teams in their natural settings, and indicators of mental workload and team dynamics derived from the data. Such a study will need to focus on the feasibility of using fNIRS+EEG for prediction and classification of multimodal data. Machine learning techniques can be implemented for mental load detection. Our preliminary based on the data presented in this thesis Section 3.1.3 showed that multimodal fNIRS+EEG classification accuracy was higher the individual modalities alone.

REFERENCES

1. White BR, Snyder AZ, Cohen AL, Petersen SE, Raichle ME, Schlaggar BL, Culver JP (2009) Resting-state functional connectivity in the human brain revealed with diffuse optical tomography. *NeuroImage* 47(1):148-156.
2. Mesquita RC, Franceschini MA, Boas DA (2010) Resting state functional connectivity of the whole head with near-infrared spectroscopy. *Biomedical optics express* 1(1):324-336.
3. Gentili RJ, Shewokis PA, Ayaz H, Contreras-Vidal JL (2013) Functional near-infrared spectroscopy-based correlates of prefrontal cortical dynamics during a cognitive-motor executive adaptation task. *Frontiers in human neuroscience* 7:277.
4. Lloyd-Fox S, Blasi A, Elwell CE (2010) Illuminating the developing brain: the past, present and future of functional near infrared spectroscopy. *Neuroscience and biobehavioral reviews* 34(3):269-284.
5. Scholkmann F, Kleiser S, Metz AJ, Zimmermann R, Mata Pavia J, Wolf U, Wolf M (2014) A review on continuous wave functional near-infrared spectroscopy and imaging instrumentation and methodology. *NeuroImage* 85 Pt 1:6-27.
6. Uglialoro A, Pfeil D, Gevorgyan T, Graber HL, Xu Y, Mangla S, Barone FC, Libien J, Charchaflieh J, Kral JG, Ramirez SA, Simpson L, Lee, DC, Barbour, R (2014) Cerebral Monitoring and Surveillance Using High-Resolution Functional

Optical Imaging. *Neurovascular Coupling Methods,* Neuromethods, eds Zhao M, Ma H, Schwartz TH (Springer New York), Vol 88, pp 307-330.

7. Durduran T, Zhou C, Buckley EM., Kim MN, Yu G, Choe R., Gaynor JW, Spray, TL, Durning S M, Mason S E, Montenegro LM, Nicolson SC, Zimmerman R A, Putt, ME, Wang J, Greenberg JH, Detre JA, Yodh AG, Licht D J (2010) Optical measurement of cerebral hemodynamics and oxygen metabolism in neonates with congenital heart defects. *Journal of biomedical optics* 15(3):037004.
8. Strangman G, Culver JP, Thompson JH, Boas DA (2002) A quantitative comparison of simultaneous BOLD fMRI and NIRS recordings during functional brain activation. *NeuroImage* 17(2):719-731.
9. Huppert TJ, Hoge RD, Diamond SG, Franceschini MA, Boas DA (2006) A temporal comparison of BOLD, ASL, and NIRS hemodynamic responses to motor stimuli in adult humans. *NeuroImage* 29(2):368-382.
10. Steinbrink J, Villringer, A, Kempf F, Haux D, Boden S, Obrig H (2006) Illuminating the BOLD signal: combined fMRI-fNIRS studies. *Magnetic resonance imaging* 24(4):495-505.
11. Kleinschmidt A, Obrig H, Requardt M, Merboldt KD, Dirnagl U, Villringer A, Frahm J (1996) Simultaneous recording of cerebral blood oxygenation changes during human brain activation by magnetic resonance imaging and near-infrared spectroscopy. *Journal of cerebral blood flow and metabolism : official journal of the International Society of Cerebral Blood Flow and Metabolism* 16(5):817-826.

12. Buzsaki G, Anastassiou CA, Koch C (2012) The origin of extracellular fields and currents--EEG, ECoG, LFP and spikes. *Nature reviews. Neuroscience* 13(6):407-420.

13. Whitham EM, Pope KJ, Fitzgibbon SP, Lewis T, Clark CR, Loveless S, Broberg M, Wallace A, DeLosAngeles D, Lillie P, Hardy A, Fronsko R, Pulbrook A, Willoughby JO (2007) Scalp electrical recording during paralysis: quantitative evidence that EEG frequencies above 20 Hz are contaminated by EMG. *Clinical neurophysiology : official journal of the International Federation of Clinical Neurophysiology* 118(8):1877-1888.

14. Goncharova, II, McFarland DJ, Vaughan TM, Wolpaw JR (2003) EMG contamination of EEG: spectral and topographical characteristics. *Clinical neurophysiology : official journal of the International Federation of Clinical Neurophysiology* 114(9):1580-1593.

15. Muthukumaraswamy SD (2013) High-frequency brain activity and muscle artifacts in MEG/EEG: a review and recommendations. *Frontiers in human neuroscience* 7:138.

16. Pope KJ, Fitzgibbon SP, Lewis TW, Whitham EM, Willoughby JO (2009) Relation of gamma oscillations in scalp recordings to muscular activity. *Brain topography* 22(1):13-17.

17. Varela F, Lachaux JP, Rodriguez E, Martinerie J (2001) The brainweb: phase synchronization and large-scale integration. *Nature reviews. Neuroscience* 2(4):229-239.

18. Greenfield LJ, Geyer JD, Carney PR (2009) *Reading EEGs: A Practical Approach* (Lippincott Williams & Wilkins, Philadelphia, PA).

19. Schomer DL, Lopes de Silva F. (2010) *Niedermeyer's Electroencephalography: Basic Principles, Clinical Applications, and Related Fields* (Lippincott Williams & Wilkins, Philadelphia, PA).

20. Grant AC, Abdel-Baki S G, Weedon J, Arnedo V, Chari G, Koziorynska E, Lushbough C, Maus D, McSween T, Mortati K A, Reznikov A, Omurtag A (2014) EEG interpretation reliability and interpreter confidence: a large single-center study. *Epilepsy & behavior : E&B* 32:102-107.

21. Srinivasan R, Winter WR, Ding J, Nunez PL (2007) EEG and MEG coherence: measures of functional connectivity at distinct spatial scales of neocortical dynamics. *Journal of neuroscience methods* 166(1):41-52.

22. Goncalves SI, Goncalves SI, de Munck JC, Pouwels PJ, Schoonhoven R, Kuijer JP, Maurits NM, Hoogduin JM, Van Someren EJ, Heethaar RM, Lopes da Silva FH (2006) Correlating the alpha rhythm to BOLD using simultaneous EEG/fMRI: inter-subject variability. *NeuroImage* 30(1):203-213.

23. Britz J, Van De Ville D, Michel CM (2010) BOLD correlates of EEG topography reveal rapid resting-state network dynamics. *NeuroImage* 52(4):1162-1170.

24. Sadaghiani S, Scheeringa R, Lehongre K, Morillon B, Giraud AL, Kleinschmidt A (2010) Intrinsic connectivity networks, alpha oscillations, and tonic alertness: a simultaneous electroencephalography/functional magnetic resonance imaging study. *The Journal of neuroscience : the official journal of the Society for Neuroscience* 30(30):10243-10250.

25. Huster RJ, Debener S, Eichele T, Herrmann CS (2012) Methods for simultaneous EEG-fMRI: an introductory review. *The Journal of neuroscience : the official journal of the Society for Neuroscience* 32(18):6053-6060.

26. Pouliot P, Tremblay J, Robert M,Vannasing P, Lepore F, Lassonde M, Sawan M, Nguyen DK, Lesage F (2012) Nonlinear hemodynamic responses in human epilepsy: a multimodal analysis with fNIRS-EEG and fMRI-EEG. *Journal of neuroscience methods* 204(2):326-340.

27. Mantini D, Perrucci MG, Del Gratta C, Romani GL, Corbetta M (2007) Electrophysiological signatures of resting state networks in the human brain. *Proceedings of the National Academy of Sciences of the United States of America* 104(32):13170-13175.

28. Goldman RI, Stern JM, Engel J, Jr., Cohen MS (2002) Simultaneous EEG and fMRI of the alpha rhythm. *Neuroreport* 13(18):2487-2492.

29. Koch SP, Koendgen S, Bourayou R, Steinbrink J, Obrig H (2008) Individual alpha-frequency correlates with amplitude of visual evoked potential and hemodynamic response. *NeuroImage* 41(2):233-242.

30. Koch SP, Steinbrink J, Villringer A, Obrig H (2006) Synchronization between background activity and visually evoked potential is not mirrored by focal hyperoxygenation: implications for the interpretation of vascular brain imaging. *The Journal of neuroscience : the official journal of the Society for Neuroscience* 26(18):4940-4948.

31. Koch SP, Werner P, Steinbrink J, Fries P, Obrig H (2009) Stimulus-induced and state-dependent sustained gamma activity is tightly coupled to the hemodynamic

response in humans. *The Journal of neuroscience : the official journal of the Society for Neuroscience* 29(44):13962-13970.

32. Roche-Labarbe N, Zaaimi B, Berquin P, Nehlig A, Grebe R, Wallois F (2008) NIRS-measured oxy- and deoxyhemoglobin changes associated with EEG spike-and-wave discharges in children. *Epilepsia* 49(11):1871-1880.

33. Giacometti P, Diamond SG (2013) Compliant head probe for positioning electroencephalography electrodes and near-infrared spectroscopy optodes. *Journal of biomedical optics* 18(2):27005.

34. Safaie J, Grebe R, Abrishami Moghaddam H, Wallois F (2013) Toward a fully integrated wireless wearable EEG-NIRS bimodal acquisition system. *Journal of neural engineering* 10(5):056001.

35. Keles HO, Barbour RL, Aghajani H, Omurtag A (2014) Investigation of neurovascular coupling from simultaneous fNIRS-EEG system using triplet holder. in *fNIRS2014* (Montreal, Canada).

36. Llinas R, Ribary U, Contreras D, Pedroarena C (1998) The neuronal basis for consciousness. *Philosophical transactions of the Royal Society of London. Series B, Biological sciences* 353(1377):1841-1849.

37. Buzsaki G, Draguhn A (2004) Neuronal oscillations in cortical networks. *Science* 304(5679):1926-1929.

38. Berger H (1929) Über das Elektroenkephalogram des Menschen. *Arch. f. Psychiat.* 87:527-570.

39. Steriade M (2001) Impact of network activities on neuronal properties in corticothalamic systems. *Journal of neurophysiology* 86(1):1-39.

40. Steriade M (2006) Grouping of brain rhythms in corticothalamic systems. *Neuroscience* 137(4):1087-1106.

41. Laufs H, Kleinschmidt A, Beyerle A, Eger E, Salek-Haddadi A, Preibisch C, Krakow K (2003) EEG-correlated fMRI of human alpha activity. *NeuroImage* 19(4):1463-1476.

42. Tyvaert L, Levan P, Grova C, Dubeau F, Gotman J (2008) Effects of fluctuating physiological rhythms during prolonged EEG-fMRI studies. *Clinical neurophysiology : official journal of the International Federation of Clinical Neurophysiology* 119(12):2762-2774.

43. Dalal SS, Zumer JM, Guggisberg AG,Trumpis M, Wong D D, Sekihara K, Nagarajan SS (2011) MEG/EEG source reconstruction, statistical evaluation, and visualization with NUTMEG. *Computational intelligence and neuroscience* 2011:758973.

44. Jobsis FF (1977) Noninvasive, infrared monitoring of cerebral and myocardial oxygen sufficiency and circulatory parameters. *Science* 198(4323):1264-1267.

45. Chance B, Zhuang Z, UnAh C, Alter C, Lipton L (1993) Cognition-activated low-frequency modulation of light absorption in human brain. *Proceedings of the National Academy of Sciences of the United States of America* 90(8):3770-3774.

46. Hoshi Y, Tamura M (1993) Dynamic multichannel near-infrared optical imaging of human brain activity. *Journal of applied physiology* 75(4):1842-1846.

47. Kato T, Kamei A, Takashima S, Ozaki T (1993) Human visual cortical function during photic stimulation monitoring by means of near-infrared spectroscopy.

Journal of cerebral blood flow and metabolism : official journal of the International Society of Cerebral Blood Flow and Metabolism 13(3):516-520.

48. Villringer A, Planck J, Hock C, Schleinkofer L, Dirnagl U (1993) Near infrared spectroscopy (NIRS): a new tool to study hemodynamic changes during activation of brain function in human adults. *Neuroscience letters* 154(1-2):101-104.

49. Zijlstra WG, Buursma, A., Van Assendelft, O.W., (2000) *Visible and Near Infrared Absorption Spectra of Human and Animal Haemoglobin determination and application* (CRC Press, Zeist, The Netherlands).

50. Huppert TJ, Diamond SG, Franceschini MA, Boas DA (2009) HomER: a review of time-series analysis methods for near-infrared spectroscopy of the brain. *Applied optics* 48(10):D280-298.

51. Lorenzo JR (2012) *Principles of Diffuse Light Propagation: Light Propagation in Tissues with Applications in Biology and Medicine* (Wspc).

52. Gervain J, Mehler J, Werker JF, Nelson CA, Csibra G, Lloyd-Fox S, Shukla M, Aslin RA (2011) Near-infrared spectroscopy: a report from the McDonnell infant methodology consortium. *Developmental Cognitive Neuroscience* 1:295-305.

53. Ferrari M, Quaresima V (2012) A brief review on the history of human functional near-infrared spectroscopy (fNIRS) development and fields of application. *NeuroImage* 63(2):921-935.

54. Delpy, D.T., Cope, M., van der Zee P, Arridge S, Wray S, Wyatt J (1988) "Estimation Of Optical Pathlength Through Tissue From Direct Time Of Flight Measurement. *Physics in medicine and biology* 33(12):1433-1442.

55. León-Carrión J and León-Domínguez U (2012) "Functional near-infrared spectroscopy (fNIRS): principles and neuroscientific applications". *P. Bright (Ed.), Neuroimaging-Methods (InTech)*

56. Eggebrecht AT, Ferradal SL, Robichaux-Viehoever A, Hassanpour MS, Dehghani H, Snyder AZ, Hershey T, Culver JP (2014) Mapping distributed brain function and networks with diffuse optical tomography. *Nature photonics* 8(6):448-454.

57. Zeff BW, White BR, Dehghani H, Schlaggar BL, Culver JP (2007) Retinotopic mapping of adult human visual cortex with high-density diffuse optical tomography. *Proceedings of the National Academy of Sciences of the United States of America* 104(29):12169-12174.

58. Pizzagalli DA (2007) Electroencephalography and high-density electrophysiological source localization. *Handbook of Psychophysiology*, ed Press CUNew York, NY), pp 56-84.

59. Kropotov JD (2009) *Quantitative EEG, Event-Related Potentials and Neurotherapy* (Elsevier, London).

60. Senhadji L, Wodey E, Claude E (2002) Monitoring approaches in general anesthesia: a survey. *Crit Rev Biomed Eng* 30(1-3):85-97.

61. Knyazev GG (2012) EEG delta oscillations as a correlate of basic homeostatic and motivational processes. *Neuroscience and biobehavioral reviews* 36(1):677-695.

62. Amzica F, Steriade M (1998) Electrophysiological correlates of sleep delta waves1. *Electroencephalography and Clinical Neurophysiology* 107(2):69-83.

63. Inanaga K (1998) Frontal midline theta rhythm and mental activity. *Psychiatry and clinical neurosciences* 52(6):555-566.

64. Asada H, Fukuda Y, Tsunoda S, Yamaguchi M, Tonoike M (1999) Frontal midline theta rhythms reflect alternative activation of prefrontal cortex and anterior cingulate cortex in humans. *Neuroscience letters* 274(1):29-32.

65. Pizzagalli DA, Oakes TR, Davidson RJ (2003) Coupling of theta activity and glucose metabolism in the human rostral anterior cingulate cortex: an EEG/PET study of normal and depressed subjects. *Psychophysiology* 40(6):939-949.

66. Klimesch W, Sauseng P, Hanslmayr S (2007) EEG alpha oscillations: the inhibition-timing hypothesis. *Brain research reviews* 53(1):63-88.

67. Yi W,Qiu S, Wang K, Qi H, Zhang L, Zhou P, He F, Ming D (2014) Evaluation of EEG oscillatory patterns and cognitive process during simple and compound limb motor imagery. *PloS one* 9(12):e114853.

68. Pfurtscheller G (2003) Induced oscillations in the alpha band: functional meaning. *Epilepsia* 44 Suppl 12:2-8.

69. Rihs TA, Michel CM, Thut G (2007) Mechanisms of selective inhibition in visual spatial attention are indexed by alpha-band EEG synchronization. *The European journal of neuroscience* 25(2):603-610.

70. Sigala R, Haufe S, Roy D, Dinse HR, Ritter P (2014) The role of alpha-rhythm states in perceptual learning: insights from experiments and computational models. *Frontiers in computational neuroscience* 8:36.

71. Klimesch W, Schack B, Sauseng P (2005) The functional significance of theta and upper alpha oscillations. *Experimental psychology* 52(2):99-108.

72. Freeman WJ (2004) Origin, structure, and role of background EEG activity. Part 1. Analytic amplitude. *Clinical neurophysiology : official journal of the International Federation of Clinical Neurophysiology* 115(9):2077-2088.

73. Tiitinen H, Sinkkonen J, Reinikainen K, Alho K, Lavikainen J, Naatanen R (1993) Selective attention enhances the auditory 40-Hz transient response in humans. *Nature* 364(6432):59-60.

74. Martinovic J, Gruber T, Muller MM (2007) Induced gamma band responses predict recognition delays during object identification. *Journal of cognitive neuroscience* 19(6):921-934.

75. Miltner W.H., Braun C, Arnold M, Witte H, (1999) Coherence of gamma-band EEG activity as a basis for associative learning. *Nature* 397(6718):434-436.

76. Niessing J, Ebisch B, Schmidt KE, Niessing M, Singer W, Galuske RA (2005) Hemodynamic signals correlate tightly with synchronized gamma oscillations. *Science* 309(5736):948-951.

77. Buzsaki G, Wang XJ (2012) Mechanisms of gamma oscillations. *Annual review of neuroscience* 35:203-225.

78. Gagnon L, Yucel MA, Cooper RJ, Boas DA (2014) Further improvement in reducing superficial contamination in NIRS using double short separation measurements. *NeuroImage* 15(85):127-135.

79. Gagnon L, Cooper RJ, Yucel MA, Perdue KL, Greve DN, Boas DA (2012) Short separation channel location impacts the performance of short channel regression in NIRS. *NeuroImage* 59(3):2518-2528.

80. Uludag K, Roebroeck A (2014) General overview on the merits of multimodal neuroimaging data fusion. *NeuroImage* 102 Pt 1:3-10.

81. Ives JR, Warach S, Schmitt F, Edelman RR, Schomer DL (1993) Monitoring the patient's EEG during echo planar MRI. *Electroencephalogr Clin Neurophysiol* 87(6):417-420.

82. Girouard H, Iadecola C (2006) Neurovascular coupling in the normal brain and in hypertension, stroke, and Alzheimer disease. *Journal of applied physiology* 100(1):328-335.

83. Claassen JA, Zhang R (2011) Cerebral autoregulation in Alzheimer's disease. *Journal of cerebral blood flow and metabolism : official journal of the International Society of Cerebral Blood Flow and Metabolism* 31(7):1572-1577.

84. Blicher JU, Stagg CJ, O'Shea J, Østergaard L, MacIntosh BJ, Johansen-Berg H, Jezzard P, Donahue MJ (2012) Visualization of altered neurovascular coupling in chronic stroke patients using multimodal functional MRI. *Journal of Cerebral Blood Flow & Metabolism* 32:2044-2054.

85. Zhou Y, Lui YW, Zuo XN, Milham MP, Reaume J, Grossman RI, Ge Y (2014) Characterization of thalamo-cortical association using amplitude and connectivity of functional MRI in mild traumatic brain injury. *Journal of magnetic resonance imaging : JMRI* 39(6):1558-1568.

86. Iraji A, Benson RR, Welch RD, O'Neil BJ, Woodard JL, Ayaz SI, Kulek A, Mika V, Medado P, Soltanian-Zadeh H, Liu T, Haacke EM, Kou Z (2015) Resting State Functional Connectivity in Mild Traumatic Brain Injury at the Acute Stage:

Independent Component and Seed-Based Analyses. *Journal of neurotrauma* 32(14):1031-1045.

87. Mayer AR, Mannell MV, Ling J, Gasparovic C, Yeo RA (2011) Functional connectivity in mild traumatic brain injury. *Human brain mapping* 32(11):1825-1835.

88. Len TK, Neary JP (2011) Cerebrovascular pathophysiology following mild traumatic brain injury. *Clinical physiology and functional imaging* 31(2):85-93.

89. Bari V, Calcagnile P, Molteni E, Re R, Contini D, Spinelli L, Caffini M, Torricelli A, Cubeddu R, Cerutti S, Bianchi AM (2012) From neurovascular coupling to neurovascular cascade: a study on neural, autonomic and vascular transients in attention. *Physiological measurement* 33(8):1379-1397.

90. Attwell D, Iadecola C (2002) The neural basis of functional brain imaging signals. *Trends in neurosciences* 25(12):621-625.

91. D'Esposito M, Deouell LY, Gazzaley A (2003) Alterations in the BOLD fMRI signal with ageing and disease: a challenge for neuroimaging. *Nature reviews. Neuroscience* 4(11):863-872.

92. de Munck JC, Goncalves SI, Huijboom L, Kuijer JP, Pouwels PJ Heethaar RM, Lopes da Silva FH (2007) The hemodynamic response of the alpha rhythm: an EEG/fMRI study. *NeuroImage* 35(3):1142-1151.

93. Moosmann M, Ritter P, Krastel I, Brink A, Thees S, Blankenburg F Taskin B, Obrig H, Villringer A (2003) Correlates of alpha rhythm in functional magnetic resonance imaging and near infrared spectroscopy. *NeuroImage* 20(1):145-158.

94. Ekstrom A, Suthana N, Millett D, Fried I, Bookheimer S (2009) Correlation Between BOLD fMRI and Theta-Band Local Field Potentials in the Human Hippocampal Area. *Journal of neurophysiology* 101(5):2668-2678.

95. Arthurs O.J, Boniface SJ (2003) What aspect of the fMRI BOLD signal best reflects the underlying electrophysiology in human somatosensory cortex? *Clinical Neurophysiology* 114(7):1203-1209.

96. Omurtag A, Abdel Baki SG, Chari G, Cracco RC, Zehtabchi S, Fenton AA, Grant AC (2012) Technical and clinical analysis of microEEG: a miniature wireless EEG device designed to record high-quality EEG in the emergency department. *Int J Emerg Med.* 5(35).

97. Abdel Baki S.G, A. O, Fenton A.A, Zehtabchi S (2011) The New Wave: time to bring EEG into the Emergency Department. *Int J Emerg Med.* 4(36).

98. Muthukumaraswamy SD (2013) High-frequency brain activity and muscle artifacts in MEG/EEG: a review and recommendations. *frontiers in human neuroscience*:00138.

99. Herrmann MJ, Ehlis AC, Fallgatter AJ (2003) Frontal activation during a verbal-fluency task as measured by near-infrared spectroscopy. *Brain Research Bulletin* 61(1):51-56.

100. Sara V. Tupaka MB, Thomas Dreslera , Tim Hahn, Lena H. Ernstb, Martin J. Herrmann, Andreas J. Fallgatter, Ann-Christine Ehlisb (2012) ifferential prefrontal and frontotemporal oxygenation patterns during phonemic and semantic verbal fluency. *Neuropsychologia*:1565-1569.

101. Schecklmann M, Ehlis AC, Plichta MM, Fallgatter AJ (2010) Influence of muscle activity on brain oxygenation during verbal fluency assessed with functional near-infrared spectroscopy. *Neuroscience* 171(2):434-442.

102. Wu L, Eichele T, Calhoun VD (2010) Reactivity of hemodynamic responses and functional connectivity to different states of alpha synchrony: a concurrent EEG-fMRI study. *NeuroImage* 52(4):1252-1260.

103. Feige B, Scheffler K, Esposito F, Di Salle F, Hennig J, Seifritz E (2005) Cortical and subcortical correlates of electroencephalographic alpha rhythm modulation. *Journal of neurophysiology* 93(5):2864-2872.

104. Sirovich L, Omurtag A, Lubliner K (2006) Dynamics of neural populations: stability and synchrony. *Network* 17(1):3-29.

105. Sirotin YB, Das A (2009) Anticipatory haemodynamic signals in sensory cortex not predicted by local neuronal activity. *Nature* 457(7228):475-479.

106. Mukamel R, Gelbard H, Arieli A, Hasson U, Fried I, Malach R (2005) Coupling between neuronal firing, field potentials, and FMRI in human auditory cortex. *Science* 309(5736):951-954.

107. Nir Y, Fisch L, Mukamel R, Gelbard-Sagiv H, Arieli A, Fried I, Malach R (2007) Coupling between neuronal firing rate, gamma LFP, and BOLD fMRI is related to interneuronal correlations. *Current biology : CB* 17(15):1275-1285.

108. Logothetis NK, Pauls J, Augath M, Trinath T, Oeltermann A (201) Neurophysiological investigation of the basis of the fMRI signal. *Nature* 412(6843):150-157.

109. Byrne A. (2012) Mental workload as a key factor in clinical decision making. Advances in Health Sciences Education 18(3):537-545.

110. Prabhu A, Smith W, Yurko Y, Acker C, Stefanis D (2010) Increased stress levels may explain the incomplete transfer of simulator-acquired skill to the operating room. *Surgery* 147:640–645.

111. Guru KA, Esfahani ET, Raza SJ, Bhat R, Wang K, Hammond Y, Wilding G, Peabody JO, Chowriappa AJ (2012) Cognitive skills assessment during robot-assisted surgery; separating the wheat from the chaff. *BJU Int* 115(1):166-174.

112. Lindauer U, Dirnagl U, Fuchtemeier M, Bottiger C, Offenhauser N, Leithner C, Royl G (2010) Pathophysiological interference with neurovascular coupling-when imaging based on hemoglobin might so blind. *Front. Neuroenergetics* 4(2):25.

113. D'Esposito M, Deouell LY, Gazzaley A (2003) Alterations in the BOLD fMRI signal with ageing and disease: a challenge for neuroimaging. *Nature Rev. Neuroscience* 4(2003):863-872

114. Zhang Y, Sun JW, Rolfe P (2012) RLS adaptive filtering for physiological interference reduction in NIRS brain activity measurement: a Monte Carlo study. *Physiological Measurement* 33(6):925

115. Center for Disease Control (CDC), "Get the Stats on Traumatic Brain Injury in the United States," 2010. [Online]. Available: http://www.cdc.gov/traumaticbraininjury/pdf/BlueBook_factsheet-a.pdf.

116. Defense Centers of Excellence for Psychological Health and Traumatic Brain Injury (DCoE) , "Portable Field-Based Devices for the Early Diagnosis of mTBI," 2010.

117. Keles HO, Barbour RL, Aghajani H, Omurtag A (2014) Multimodality mapping approach for evolving functional brain connectivity patterns: A fNIRS-EEG study. *in OSA Biomed 2014 (Miami).*